Active and stable ceria-zirconia supported molybdenum oxide catalysts for cyclooctene epoxidation: Effect of the preparation procedure

~~Study of the effect of preparation procedure on the formation of active and stable ceria-zirconia supported molybdenum oxide catalysts for cyclooctene epoxidation~~

Active and stable ceria-zirconia supported molybdenum oxide catalysts for cyclooctene epoxidation: effect of the preparation procedure

Formattato: Colore carattere: Automatico

R. Turco[1], B. Bonelli[2], M. Armandi[2], L. Spiridigliozzi[3], G. Dell'Agli[3], F.A. Deorsola, S. Esposito[2]*, M. Di Serio[1,4]

[1]Università degli Studi di Napoli Federico II, Dipartimento di Scienze Chimiche, Via Cintia, I-80126 Napoli, Italy.

[2]Dipartimento di Scienza Applicata e tecnologia e Unità INSTM Torino-Politecnico Corso Duca degli Abruzzi, 24 – I-10129 Torino, Italy.

[3]Dipartimento di Ingegneria Civile e Meccanica Università degli Studi di Cassino e del Lazio Meridionale Via G. Di Blasio, 43 – I-03043 Cassino (FR), Italy.

[4] International Research Organization for Advanced Science and Technology (IROAST), University of Kumamoto, 860-8555 Kumamoto, Japan.

Corresponding author:

Serena Esposito: serena_esposito@polito.it

Abstract

$Ce_{0.75}Zr_{0.25}O_2$ supports were prepared by precipitation in the presence of either ammonia or urea as precipitating agents. Mo(VI) oxide was dispersed onto the supports by either co-precipitation or wet impregnation, using ammonium eptamolybdate tetrahydrate as the Mo precursor. In all the cases, the nominal Mo content was 6.6 wt.%, selected to be under the value of the reported monolayer capacity of molybdenum oxide. The catalysts prepared by using ammonia as precipitating agent showed a superior catalytic activity in the cyclooctene epoxidation, with cumene hydroperoxide as oxidizing agent. The stability of the catalysts was confirmed by multiple runs and the absence of leaching was verified according to the Sheldon method. Physico-chemical characterization of the catalysts revealed that urea promotes the formation of hydrated cerium(III) oxycarbonate, which likely hampers a homogeneous distribution of active MoO_x species that, conversely, are fairly stabilized on the support when ammonia is used as precipitating agent.

Keywords: molybdenum-containing catalysts; epoxidation; ceria-zirconia solid solution; co-precipitation and impregnation methods; precipitating agent

1. Introduction

In recent years, there has been a great deal of interest in the catalytic partial oxidation of alkenes to produce epoxides, as the latter are versatile and useful intermediates in the production of fine chemicals and/or pharmaceuticals. [1-8].

The reaction can be carried out by using different oxidizing agents, namely peroxycarboxylic acids [9-11], hydrogen peroxide [12], hydroperoxides [13-15]. Peroxycarboxylic acids are obtained *in situ* by using mineral acids as catalysts, according to the Prileshajew method [16-17], which is far from being an environmentally benign one, since the employed organic acid is not recovered at the end of the reaction, and, in the case of formic acid, is degraded to CO_2 and H_2 [10]. From the point of view of the environmental impact, hydrogen peroxide (H_2O_2) is the most efficient oxidizing agent, but it is applied industrially only to the production of propylene oxide [18], since, so far, only titanium silicalite TS-1 has shown sufficient activity, stability and selectivity towards alkene epoxidation by H_2O_2. Nevertheless, its pores are too small (0.51-0.56 nm) to allow a facile diffusion of alkenes larger that propylene [18].

An intense research is devoted to find a heterogenous catalytic system that can catalyze the alkenes epoxidation by H_2O_2 with high selectivity and stability to leaching [19]. However, the industrial production of propylene oxide is also carried out by employing, as oxidizing agents, more environmentally benign hydroperoxides in the presence of either homogeneous or heterogeneous catalysts [19]. Such method also allows the epoxidation of heavier alkenes [19].

To this end, Mo(VI) complexes are acknowledged to be powerful catalysts in homogenous phase for the epoxidation of alkenes by hydroperoxides, but the use of a heterogeneous catalyst could further improve the economy of industrial applications due to lower requirements in terms of work-up, product isolation and purification procedures [20-252]. The development of simple methods to

synthesise supported Mo catalysts would offer a significant solution to grasp the need of more sustainable epoxidation processes.

Several attempts and strategies to prepare Mo-based heterogeneous catalysts focused on post synthesis methods, either by direct grafting Mo complexes or by using a linker between the catalyst and the support [13, 2~~36~~-31~~25~~]. Moreover, many papers have been devoted to the use of polymers as supports [32-34~~26, 27~~]. Such approaches suffer from the complexity of the catalyst synthesis, the related high costs and, in many cases, from low chemical and mechanical stability [6, 32~~26~~].

Mo-containing amorphous silicates were prepared by an acid-catalysed simple sol–gel process, by using $Mo(OiPr)_5$ (Mo(V) isopropoxide) and $MoO_2(acac)_2$ as Mo oxide precursors: in the case of $MoO_2(acac)_2$ derived catalysts, homogeneous catalysis was observed due to the leaching of some active species, whereas more promising results in alkenes epoxidation were obtained by using $Mo(OiPr)_5$ as precursor, albeit the Mo content in the catalysts dropped after the third catalytic run [35~~28~~].

As a possible solution to Mo-leaching, Hyeon et al. [36~~29~~] proposed the coating of dense silica-coated magnetite nanoparticles with molybdenum oxide nanoparticles embedded within a mesoporous silica shell. The so-obtained epoxidation catalyst is easily recovered by exploiting its magnetic properties, but its production is the result of a demanding multi-step procedure involving the sol-gel synthesis of the two different silica layers and the impregnation with ammonium molybdate precursor. The nanocomposite was then reduced in a flowing mixture of H_2 and N_2 (1:1) at 500 °C for 12 h to produce MoO_2 nanoparticles. A simpler synthesis of ultra-small MoO_3 nanoparticles supported on different oxide nanospheres (SiO_2, TiO_2 and ZrO_2) by reverse micelles micro-emulsion method was reported by Prakash Chandra et al. [3~~0~~] MoO_3/SiO_2 catalysts gave the best results in the catalytic oxidation of cyclooctene, whereas very low activity was observed with both MoO_3/ZrO_2 and MoO_3/TiO_2. Such different catalytic behaviours were related to the different degree of dispersion of MoO_3 oxide nanoparticles at the surface of the nanospheres.

High yields and 99 % selectivity in cyclohexene epoxidation by tert-butyl hydroperoxide were obtained by using Mo-ZrO_2 catalyst [381]. However, a severe leaching of the catalytic species was observed, and the catalytic activity of Mo-ZrO_2 was interpreted as due to a combination of both heterogeneous and homogeneous catalysis. No yield loss upon recycling was observed only when molybdenum(VI) oxide was deposited on a more complex ~~platform~~support, *i.e.* the Zr6 node of the mesoporous metal − organic framework NU-1000 [381].

Since the immobilization of highly active Mo species on a proper support is still a challenge from a practical point of view, this paper aims at exploring the use of ceria-zirconia as a support for active and stable molybdenum oxide. Although Zr-doped ceria has grabbed tremendous attention over the past decades for its unique features as heterogeneous catalyst, to our knowledge, it has never been used to disperse active Mo-based catalytic species for epoxidation reactions. To this respect, some of us carried out several studies concerning the wet chemical synthesis of zirconia-based ceramics and ceria-based ceramics, also by precipitation from aqueous solution [392-42~~35~~]. Here, some simple co-precipitation routes have been selected either for the direct synthesis of Mo-supported catalysts (MoO_x-$Ce_{0.75}Zr_{0.25}O_2$) or of the bare ceria-zirconia support~~,~~ followed by wet impregnation of the Mo phase (MoO_x/ $Ce_{0.75}Zr_{0.25}O_2$ catalysts).

The activity and reusability of the prepared catalysts in cyclooctene epoxidation with cumene hydroperoxide are assessed and the differences that may be ascribed to the preparation route and/or from specific Mo-support interactions discussed. Attention is paid to the study of molybdenum leaching (Mo) from the catalyst supported by ceria-zirconia through an adequate test and analysis of the reaction solution, blank test. Finally, decommissioning was examined by re-use tests. The effect of the precipitating agent (either urea or ammonia) on both dispersion and activity of the MoOx are investigated by means of a detailed physico~~physic~~-chemical characterization of the structural and surface properties of the samples. Attention is devoted to their acidic properties (types, abundance

and strength of the acid sites), as studied by means of a combined NH_3-TPD and IR spectroscopy investigation.

2. Experimental Section

2.1 Catalysts Synthesis

Cerium(III) nitrate hexahydrate ($Ce(NO_3)_3 \cdot 6H_2O$, Carlo Erba, Italy), zirconium(IV) oxychloride octahydrate ($ZrOCl_2 \cdot 8H_2O$) and ammonium eptamolybdate tetrahydrate ($(NH_4)_6Mo_7O_{24} \cdot 4H_2O$) were used as precursors of the catalysts. Either an ammonia solution (NH_3 solution 30%, Carlo Erba, Italy) or urea ($CO(NH_2)_2$ 99.5% Carlo Erba, Italy) were selected as precipitating agents [43~~36~~].

Two series of samples were prepared, in that the desired amount of Mo was either directly co-precipitated along with the ceria-zirconia matrix (single step procedure, MoO_x-$Zr_{0.25}Ce_{0.75}O_2$) or added by wet impregnation on the previously co-precipitated support (two-step procedure, MoO_x/ $Ce_{0.75}Zr_{0.25}O_2$). In all the cases, the nominal Mo content was 6.6 wt.%.

Additionally, bare support powders (Ce/Zr molar ratio equal to 3, nominally corresponding to the chemical composition: $Ce_{0.75}Zr_{0.25}O_2$) were prepared by single step co-precipitation, either at room temperature (when ammonia solution was used as precipitating agent) or at high temperature (when urea was used as precipitating agent).

2.1.1 Single step co-precipitation

Regarding samples prepared by single step co-precipitation, a typical synthesis procedure can be described as follows. Firstly, proper amounts of cerium and zirconium precursors (Ce/Zr molar ratio equal to 3) were dissolved in deionized water, until a 0.1 M cations total concentration was reached (solution A). Then, a proper amount of ammonium eptamolybdate was added to solution A. Two other solutions containing, respectively, either diluted NH_3 solution (≈1 M NH_3, solution B) or

urea (solution C) were prepared. All the starting solutions were vigorously stirred for 15 min to ensure full precursors dissolution and homogenization.

When ammonia was the precipitating agent, an appropriate amount of solution B was slowly added to solution A in a total reflux apparatus, in order to have a large excess of the base, at high temperature (≈90°C) to allow Mo precipitation. After mixing solutions A and B, a co-precipitate of the Mo-containing powder precursor (co-precipitation at high temperature) began to form.

When urea was the precipitating agent, the amount of solution C necessary to reach a molar ratio urea/cation = 20 (again, to ensure a large excess of base) was added to solution A at r.t. and, then, the resulting solution was kept under vigorous stirring and heated up to T > 83°C. In fact, at temperatures exceeding 83°C, urea decomposes in the solution into NH_4^+ and CO_3^{2-} ions accounting for a slow and homogeneous pH increase that favors the co-precipitate formation by avoiding localized reactants distribution.

In all the cases, the as-obtained suspensions underwent a short ageing step (in the order of several minutes) and then the co-precipitates were filtered, repeatedly washed with both deionized water and ethanol, and finally dried overnight at 80°C.

2.1.2 Wet impregnation

As for samples prepared by single step co-precipitation, a typical two step synthesis firstly involved the dissolution of cerium and zirconium precursors into solution A, the preparation of the two precipitating solutions (solution B, NH_3, and solution C, urea), and the co-precipitation of the support powders either at room temperature (when ammonia solution was used as precipitating agent) or at T > 83 °C (when urea was used as precipitating agent). Afterwards, the samples prepared by wet impregnation underwent an additional step, in that the proper amount of Mo was impregnated on the co-precipitated support. In this case, the support powder was contacted with a concentrated solution of ammonium eptamolybdate (solution D), and the resulting suspension was slowly heated under

vigorous stirring until the complete evaporation of water. The as-obtained impregnated powders were subsequently dried overnight at 80 °C to remove any residual moisture.

Finally, all the precursor powders underwent calcination at 450 °C for 1 h to obtain the investigated catalysts. All the prepared samples have a nominal molybdenum content equal to 6.6 wt.% and are listed in Table 1, which summarizes also the synthesis condition.

2.2 Catalysts Characterization

X-ray Diffraction (XRD) patterns of the powders were measured on an X'Pert Philips diffractometer (PANalytical B.V.), using Cu Kα radiation in the 20°–100° 2θ range (step width = 0.02° 2θ; time per step 1 s). The obtained diffraction patterns were indexed according to the PDF-2 Release 2002 database. The lattice parameter of fluorite phase was calculated by unit cell refinement by using the software UnitCell [~~44~~37]. The crystallite size (nm) was calculated from the reflection of (111) of fluorite phase at 2θ of about 28.5 using the Scherrer equation.

N_2 adsorption/desorption isotherms at -196 °C were measured on *ca*. 100 mg powder sample previously outgassed at 250 °C for 3 h to remove water and other atmospheric contaminants (QuantachromeAutosorb 1 instrument): samples specific surface area (SSA) was calculated according to the BET (Brunauer-Emmett-Teller) method; the total pore volume was determined from the adsorbed amount at P/P^0 = 0.98 (desorption curve); micropore volume was calculated by applying the *t*-plot method; the pore size distribution was calculated by applying the Barrett–Joyner–Halenda (BJH) to isotherms desorption branch.

NH_3-TPD (Temperature Programmed Desorption) analysis was carried out in a quartz bed-fixed reactor connected to a NH_3 ND-IR (Non- Dispersive Infra-Red) ABB Uras 14 gas analyzer. In each experiment, *ca*. 200 mg sample was pre-treated under N_2 flow (100 mL min^{-1}) for 60 min at 500 °C (temperature ramp = 10 °C min^{-1}). Then, a mixture of 2000 ppm NH_3 in He (400 mL min^{-1}) was fed into the reactor at 100 °C for the adsorption run, which lasted until the NH_3 concentration value reached the initial one. The desorption run was performed under N_2 flow (400 mL min^{-1}) firstly at

r.t. to remove the loosely physisorbed fraction, and subsequently by increasing the temperature up to 600 °C (temperature ramp = 5 °C min^{-1}).

For IR measurements, the calcined powders were pressed ~~as~~into thin self-supporting wafers (*ca.* 20 mg cm^{-2}) and ~~were~~ heated under vacuum (~~p~~residual pressure below ~~<~~ 0.1 Pa) up to 673 K (ramp 5 K min^{-1}) in a homemade quartz cell equipped with (IR transparent) KBr windows. In order to avoid Ce^{4+} reduction, $O_{2(g)}$ (4000 Pa) was introduced into the cell, which was kept at 673 K for 30 min and subsequently cooled (in $O_{2(g)}$~~oxygen~~) to 393 K. Finally, the cell was cooled under vacuum to room temperature (r.t.) ~~F.~~). ~~Then,~~ or in situ adsorption measurements, ~~the~~the cell was sealed and connected to a specific vacuum line ~~for in situ adsorption measurements.. The~~ IR spectra were recorded at 2 cm^{-1} resolution~~s~~ on a BRUKER EQUINOX-55 spectrometer, ~~equipped with a mercury~~ cadmium telluride (MCT) cryodetector. IR spectra were recorded ~~by~~after dosing ~~at r.t.~~ increasing amounts of NH_3 (1-2000 Pa equilibrium pressure range) on the pre-treated samples at r.t., and subsequently by outgassing under vacuum ($p < 0.1$ Pa) at r.t. (in situ), 353, 433, and 513 K. For thermal desorption, the cell (kept under vacuum) was *i)* moved to the vacuum line used for the above described heat treatment; *ii)* heated under vacuum at the desired temperature; *iii)* cooled again to r.t.; iv) and finally brought back to the IR spectrophotometer for spectra acquisition. In order to better allow comparison, the IR spectra were normalized with respect ~~to the pellet density~~to unit specific weight. The difference spectra ~~in Figure 9~~ were obtained by subtracting the IR spectrum of the naked wafer (before NH_3 adsorption/desorption). High purity gases (O_2 6.0 purity and NH_3 5.5 purity) were purchased from SIAD

~~For IR measurements, the powders were pressed as thin self-supporting wafers (*ca.* 20 mg cm^{-2}) and were heated under vacuum up to 673 K (ramp 5 K min^{-1}) in a homemade quartz cell equipped with (IR transparent) KBr windows. Then, in order to avoid Ce^{4+} reduction, O_2 (4000 Pa) was introduced into the cell, which was kept at 673 for 30 min and subsequently cooled (in oxygen) to 393 K. Finally, the cell was cooled under vacuum to room temperature (r.t.). The IR spectra were recorded at 2 cm^{-1} resolutions on a BRUKER EQUINOX-66 spectrometer equipped with a mercury~~

Formattato: Colore carattere: Automatico

Formattato: Colore carattere: Automatico

Formattato: Colore carattere: Automatico

Formattato: Colore carattere: Automatico

Formattato: Colore carattere: Automatico

Formattato: Colore carattere: Automatico

Formattato: Colore carattere: Automatico

Commentato [LS1]: Visto lo spostamento di paragrafo, toglierei qui il riferimento alla figura

~~cadmium telluride (MCT) cryodetector. IR spectra were recorded by dosing at r.t. increasing amounts of NH_3 (1-2000 Pa equilibrium pressure range) on the pre-treated samples, and subsequently outgassing at r.t., 353, 433, and 513 K. In order to better allow comparison, the IR spectra were normalized with respect to the pellet density. The difference spectra in Figure 9 were obtained by subtracting the IR spectrum of the naked wafer (before NH_3 adsorption/desorption).~~

Microstructure and chemical composition of the samples were investigated by Field Emission Scanning Electron Microscopy (FESEM). Pictures were taken on a ZEISS Supra 40 FESEM instrument equipped with an Energy Dispersive X-ray (EDX) probe used to determine semi-quantitatively the samples chemical composition by a raster scan of ~ 0.05 mm^2 of sample surface. Raman spectra were acquired on a Renishaw InVia Reflex micro-Raman spectrometer (Renishaw plc, Wotton-under-Edge, UK) equipped with a cooled CCD camera. The Raman source was a diode laser (lex = 514.5 nm), and the inspection occurred over pelletized samples to ensure a "flat" surface, through a microscope objective (50X), in backscattering light collection. The following conditions were employed to collect each spectrum: 1mW laser power, 5 s of exposure time and 4 accumulations.

2.3 Catalytic Tests

The epoxidation reaction of cyclooctene was chosen for the activity study as it proceeds with the formation of corresponding epoxide without production of by-products, according to the reaction reported in scheme 1:

The catalytic activity in the cyclooctene epoxidation with cumene hydroperoxide as oxidant was assessed as follows. Epoxidation reactions were carried out in a round-bottom glass batch reactor, put in an oil bath, equipped with a condenser and thermometer, and a magnetic bar for vigorous stirring (300 rpm), under nitrogen flow. In a typical experiment, 300 mg of catalyst and 9.78 g of cyclooctene (Fluka, 98 wt%) were loaded and mixture was heated up to 80° C under vigorous stirring. At that temperature, 24.5 g of cumene hydroperoxide (Sigma, 80 wt% in cumene) were slowly added drop by drop through a syringe. Then, the temperature was kept constant (≈80 °C) and the reaction was

Formattato: Rientro: Prima riga: 0"

conducted up to 24 h. Samples were withdrawn at different reaction times and cooled to room temperature by quenching them in cold water. Then, the organic phase of the reaction mixtures was rapidly analysed by gas chromatography (HP 5890) using a capillary column (Chrompack CP Wax; 100% polyethyleneglycol; 30 m × 0.25 mm i.d.; film thickness: 0.25 µm) and a FID detector.

Possible leaching phenomena of the active species into the liquid phase under operating conditions have been verified by removing the catalyst from the reaction mixture (by filtration) 150 min after from the start of the reaction, and determining the residual conversion for additional 150 min.

For each molybdenum content measurement, an amount of sample (about 0.3 g) was mineralized by microwave-assisted oxidative acid digestion with addition of 9 ml of HNO_3 and 1 ml of ultrapure H_2O_2, in a ~~. The~~ Mars microwave digestion system ~~used is Mars from th~~(e ~~CEM~~ company). ~~The dD~~.

After the acid digestion treatment, the mixture was recovered and brought a final volume of 25 ml with 2 wt% HNO_3 ~~2wt%~~ solution. ~~.~~The samples were diluted 1:10 with 2 wt% HNO_3 ~~HNO_3 2%~~ for the subsequent analyzes. Elemental analysis was performed ~~using~~by inductively coupled plasma - mass spectrometry (ICP-MS, Aurora M90, Bruker). ~~The~~ Elements concentrations ~~of the elements~~ were determined with respect to a calibration curve. Detection limits (LOD) and limits of quantification (LOQ) were calculated taking into account three and ten times the standard deviation of ten replicates on a blank sample

Formattato: Inglese (Regno Unito)

Commentato [BB2]: Cosa vuol dire?

3. Result and Discussion

For the sake of clarity, Table 1 reports all the as-synthesized ceria zirconia supported molybdenum samples, along with their samples code and synthesis conditions.

~~3.1 Catalytic tests~~

The epoxidation reaction of cyclooctene was chosen for the activity study as it proceeds with the formation of corresponding epoxide without production of by-products, according to the reaction reported in scheme 1:

Then, epoxycycloctane is only product for this reaction [38].

Fig. 1 shows the profiles of cyclooctene conversion versus time for the Mo-containing catalysts reported in Table 1 (the bare supports were not active)

High cyclooctene conversions were obtained in presence of the catalysts prepared by using ammonia, in that 94 % and 85 % conversion was reached after 24 h with I-MoCeZr-A and C-MoCeZr-A catalyst, respectively. Both catalysts obtained by using urea, regardless the type of synthesis method adopted (i.e. impregnation or co-precipitation), show a poor activity.

Moreover, much larger TOF (turn-over frequency) values (Table 2) were obtained when ammonia was used as the precipitating agent, with a large difference between I-MoCeZr-A and C-MoCeZr-A. Such different catalytic results have to be ascribed to markedly different physico-chemical properties (*vide infra*).

The turn-over frequency per mol of molybdenum has been calculated as the cyclooctene consumption rate referred to the mole of molybdenum, eq. 1

$$TOF = \frac{1}{n_{Mo}} \frac{dn_{cyct.}}{dt} \quad (1)$$

According to the literature, the oxidation reaction is promoted in presence of Lewis acid sites [39-40], and medium strength Lewis centres are commended as the most active in epoxidation [38]. With this type of catalysts, the presence of Lewis acid sites is due to surface Mo species, in particular to isolated molybdenyl species that are depicted in literature as the most active Lewis acid sites in epoxidation [41-43].

The measured TOF with I-MoCeZr-A is comparable to that reported by Arnold et al. [28] for Mo/SiO_2 catalyst that, however, showed leaching issue (at 80 °C from fig. 2 of [28] it is possible to calculate a TOF of about 0.34 s^{-1}). More recently, Shen et al. [13] reviewed the progress of molybdenum-based

~~catalysts and the TOF reported for oxides (SiO_2, ZrO_2, TiO_2) supported molybdenum active species are lower with respect to ones of I-MoCeZr-A and C-MoCeZr-A.~~

~~In this work, the possible leaching of active species into the liquid phase under operating conditions was verified according the method reported by Sheldon [44], *i.e.* by removing the catalyst from the reaction mixture by filtration after 150 min from the start of the reaction, and by determining the residual conversion for additional 150 min. For each catalyst, almost no cyclooctene conversion in the filtrate was detected after the catalyst removal, providing a very strong evidence that such materials act as real heterogeneous catalysts. Moreover, the almost total absence of Mo leaching was confirmed by ICP spectroscopic analysis carried out on the reaction solution, where a concentration of Mo less than 30 ppm was detected.~~

~~From the point of view of possible industrial applications, catalyst stability is a crucial issue and, therefore, with the most active, catalysts stability was assessed by performing three runs, as follows: after each run, the solid was separated by filtration and directly reused for a new run, without washing, the corresponding results being reported in Table 3. Again, any possible leaching phenomenon was excluded by ICP analysis of the reaction solution.~~

~~With both the catalysts, the activity loss can be considered limited, as no washing was performed: such phenomenon can indicate that the catalysts are quite stable and are comparable to other catalysts obtained by more complicated synthesis and where chlorinated solvent were used in the reaction [13]. As a whole, both the I-MoCeZr-A and C-MoCeZr-A samples behave as true heterogeneous catalysts, with no leaching and good stability. The observed reduction in final conversion could be due to the blocking of catalytic sites by fouling [28], as the powders were not pre-treated (solvent washing or calcination) before each reuse cycle.~~

3.~~2~~1 Microstructural characterization: XRD and Raman spectroscopy

3.~~2~~1.1 Catalysts prepared using ammonia

The XRD patterns (Fig. S1) of the as-synthesized samples (*i.e.* not calcined), C-MoCeZr-A and I-MoCeZr-A samples indicate the presence of partially crystallized product with fluorite structure, and nanometre crystallites (estimated size in the ~~range~~ 5-10 nm range), in agreement with the general behaviour of CeO_2-based precipitates, which exhibit a strong tendency to crystallize even at room temperature [45]. The peaks position of both patterns in Fig. S1 is very close to the theoretical position of the peaks in cerianite (ICDD card. No. 34-394), thus suggesting that the crystalline fluorite phase in those samples is practically pure CeO_2, whereas both the Zr-containing precipitates (very likely a hydrated zirconium oxide) and the Mo-containing precipitate are amorphous. Furthermore, the presence of ~~a~~ residual amorphous cerium (oxo) hydroxide cannot be excluded.

The XRD patterns of the I-MoCeZr-A and C-MoCeZr-A catalysts and of the support (C-CeZr-A) calcined at 450 °C are reported in Fig. 12~~2~~. The patterns of the catalysts are very similar to each other and all show the fluorite peaks, though shifted towards higher 2θ angles with respect to cerianite, with a consequent decrease of the lattice parameter *a* (Table 24), in agreement with a partial substitution of larger Ce^{4+} cations (r_{Ce4+} = 0.97 Å in 8-fold coordination) by smaller Zr^{4+} cations (r_{Zr4+} = 0.84 Å in 8-fold coordination). With respect to the solid solution having the same nominal Ce/Zr ratio (*i.e.* $Ce_{0.75}Zr_{0.25}O_2$, ICDD card No. 28-271), the peaks are observed at lower 2θ angles, likely due a slightly lower degree of isomorphic substitution by Zr^{4+} with respect to the nominal zirconium content: accordingly, a slightly larger lattice parameter was calculated with respect to the solid solution (Table 24). The absence of any peak related to MoO_x phases suggests that Mo species are highly dispersed onto the support, likely as amorphous MoO_x oxides [46].

Finally, a careful inspection of the XRD patterns in Fig. 12~~2~~ reveals the presence of some peak asymmetry on the right hand of the most intense fluorite peaks (asterisk), which could be attributed to the presence of tetragonal zirconia (*t*-ZrO_2, ICDD card No. 50-1089). According to this hypothesis, a minor part of zirconium crystallizes into *t*-ZrO_2, in agreement with the fact that, when starting from amorphous nanosized particles, *t*-ZrO_2 forms first [4235, 47]. The formation of *t*-ZrO_2 ~~phenomenon~~ seems more pronounced in the impregnated sample. Finally, the XRD patterns of the C-CeZr-A

support resemble those of the Mo-doped samples and indicate that a solid solution forms, especially if Mo does not interfere with the dissolution of the zirconia into the ceria phase.

The Raman spectra of the C-CeZr-A support and of the I-MoCeZr-A and C-MoCeZr-A catalysts are reported in Fig. 23, where the most intense band is readily assigned to the first order Raman active F_{2g} mode of the CeO_2 fluorite structure, corresponding to the symmetrical stretching vibration of CeO_8 units, which occurs at 461 cm^{-1} in pure CeO_2. This mode is broad, asymmetric, and shifted to lower wavenumbers as compared to the single-crystal value mode [48, 49]. The F_{2g} mode (Fig. 23) is slightly blue-shifted to 463 cm^{-1} (both C-MoCeZr-A and C-CeZr-A) and to 466 cm^{-1} (I-MoCeZr-A). A blue-shift of the F_{2g} band is in agreement with a lattice contraction due to the isomorphic substitution of Zr^{4+} ions into the CeO_2 fluorite structure. The FWHM (Full Width Half Maximum) of the peak is 20, 25 and 30 cm^{-1} with I-MoCeZr-A, C-CeZr-A and C-MoCeZr-A, respectively: the broadening of the F_{2g} peak could be related to the structural disorder upon isomorphic substitution, a process that affects the order in the distribution of the various cations in the lattice [50, 51] and/or the concomitant lowering of the primary crystallite [52, 53]. Nonetheless, one of the vibrations of *t*-ZrO_2 occurs in the same region (*vide infra*), and, thus, so the interpretation of such FWHM is not straightforward.

The Raman spectrum of the support (black curve, Fig. 23) clearly shows a broad component around 600 cm^{-1}, more intense with respect to the two Mo-containing catalysts. In the literature, such band has been attributed to intrinsic defects and oxygen displacements, lowering the cubic symmetry of CeO_2 fluorite structure [52, 53]; its intensity usually increases with a progressive deformation of the lattice, resulting in the creation of defects and/or oxygen vacancies [50, 51]. Here, the band decreases in intensity in the Mo-containing catalysts, likely related to latter process, with a small difference in the two samples, indicating that somehow the MoOx units somehow favour the vacancies suppression. When MoO_3 is dispersed on a pure CeO_2 surface, oxygen anions preferentially occupy the anion vacancies on the (111) planes of the support, displacing the basic hydroxyl groups at the surface of CeO_2 [54-57]. When Mo-loading reaches the monolayer capacity, part of the cation

vacancies is occupied by Mo cations and all the anion vacancies are occupied by the corresponding oxygen anions, with formation of a close-packed monolayer of oxygen anions at the surface [56]. Therefore, the dispersion of MoOx on oxide support is driven by the shielding effect of the accompanying oxygen. [55, 58].

The final state of Mo-species can be further assessed by inspection of the 700-1100 cm^{-1} range [59, 60], where a band envelope is observed in the Mo-containing catalysts (red and green curves in Fig. 23). In the literature, bands at 800–830 and 920–970 cm^{-1} are assigned to the asymmetric stretching of Mo–O–M bridges (where M = Mo, Ce or Zr) and to the stretching of terminal Mo=O groups in surface molybdate species, respectively. The position of the Mo=O Raman band is usually shifted to higher wavenumbers (cm^{-1}) as the polymerization degree increases (being usually found below 955 cm^{-1} with dispersed polymolybdates and at 998 cm^{-1} for crystalline MoO_3 [61-62]), but is also affected by the kind of support. Due to the different radius of Ce^{4+} and Zr^{4+}, indeed, the Mo=O bond length in Mo/CeO_2 systems is longer than that in Mo/ZrO_2, and so the Raman shift of Mo=O is lower when Mo is supported on CeO_2 than on ZrO_2. Wan et al. [58] reported that, in Mo supported on CeO_2 and ZrO_2, the band due to the asymmetric stretching of Mo–O–support is at *ca*. 820 and 830 cm^{-1}, respectively, whereas the Mo=O band is at *ca*. 921 and 933 cm^{-1}, respectively. The Mo=O band occurs at 945 and 950 cm^{-1} in I-MoCeZr-A and C-MoCeZr-A, respectively, indicating that the degree of polymerization is still low, and/or that Mo-species are sitting in slightly different environment.

3.21.2 Catalysts prepared by using urea

The XRD patterns of the as-synthesized support (Fig. S2) showed that even without calcination it was well crystallized, showing only the characteristic peaks of hydrated cerium(III) oxycarbonate, $(Ce_2O(CO_3)_2 \cdot H_2O$, ICDD card No. 43-602), with peak positions very close to theoretical values.

Moreover, no peaks ascribable to Zr-containing phases were detected, indicating that Zr-based compounds were amorphous.

After calcination at 450 °C (Fig. 34) the support (i.e. when Mo is not present) shows peaks ascribable to two phases, namely cerianite (circles) and *t*-ZrO_2 (asterisks): calcination of the support leads to thermal decomposition of $Ce_2O(CO_3)_2 \cdot H_2O$, whereas the Zr-containing amorphous precipitate crystallizes into *t*-ZrO_2. Conversely, the XRD patterns of the calcined I-MoCeZr-U and C-MoCeZr-U do not present any trace *t*-ZrO_2 and show, in both cases, only the peaks of a fluorite-like phase (Fig. 3), the corresponding values of the ~~a~~ lattice parameter *a* (Table 2) being very close to those of cerianite, ~~-~~suggesting that dissolution of Zr^{4+} in the fluorite lattice occurs in ~~a~~ very small amount.

Formattato: Tipo di carattere: Corsivo

Formattato: Apice

Interestingly, the obtained results indicate that the phase transformation occurring during calcination is strongly affected by the presence of Mo.

Some of us showed that the crystallization of amorphous hydrated zirconium oxide is characterized by a sharp exothermic peak at 420-440°C [392] and so, notwithstanding calcination at 450 °C, the presence of Mo species seems to hamper the phase transition, likely by interacting with the zirconium phase [63-64].

Fig. S3 reports the XRD patterns of both I-MoCeZr-U and C-MoCeZr-U further treated at 600 °C, showing the presence of the peaks due to *t*-ZrO_2.

As a whole, with urea as precipitating agent, $Ce_2O(CO_3)_2 \cdot H_2O$ obtained at room temperature thermally decomposes at 450 °C (with consequent cerium oxidation and formation of the fluorite-like structure). The crystallization of *t*-ZrO_2 occurs almost simultaneously upon calcination and, consequently, only a very small amount of zirconium (if any) can dissolve into the ceria fluorite lattice. These results are in agreement with the findings of Tsoncheva et al., who observed phase segregation of ZrO_2 ~~phase~~ in samples prepared by coprecipitation with urea [48].

On the contrary, in the presence of ammonia, fluorite CeO_2 was already partially crystallized during the co-precipitation step, and thus the dissolution of zirconium into the fluorite lattice was favored. Besides its possible crystallization in the tetragonal form, the as-precipitated zirconium compound is

subjected to two different key drivers that determine its final allocation: requisition by the Mo-containing species or dissolution into the ceria cubic lattice. Such transformations are supposed to have remarkable influence on the final catalytic performance *(vide infra)*, as the Mo species and their coordination can determine the activity of the catalysts, which was markedly higher for the samples prepared by using ammonia.

Fig. 45 reports the corresponding Raman spectra: besides the main band due to the F_{2g} mode, the Raman spectrum of the support shows additional bands at 145, 255 and 319 cm^{-1}, which are characteristic of *t*-ZrO_2, although the exact peak positions may vary with zirconia content, particle size and different annealing temperature [65]. With *t*-ZrO_2, other two Raman bands are expected: a peak at about 460 cm^{-1}, that here likely overlaps to the F_{2g} mode of CeO_2 (*vide supra*), being also less intense than the peak at 307 cm^{-1} [51].

Raman spectra of *t*-ZrO_2 also show tetragonal phase-like lattice distortions and their associated defects with the highest frequency at about 650 cm^{-1} accompanied by a low-frequency shoulder, at around 620 cm^{-1} [53], here superposed to the band at 600 cm^{-1} assigned to CeO_2 defects. The Raman spectra of C-MoCeZr-U and I-MoCeZr-U show the main peak at 462 cm^{-1} with no shift with respect to the support C-CeZr-U, indicating that ~~the~~ formation of the solid solution is hampered by the presence of Mo, in agreement with XRD analysis. Moreover, the presence of Mo likely leads to the formation of amorphous precipitates, with formation of *t*-ZrO_2 occurring only at higher temperature~~s~~ (Fig. S3). The Mo=O stretching band occurs at 930 and 919 cm^{-1} with I-MoCeZr-U and C-MoCeZr-U, respectively, indicating the presence of ~~small~~ oligomeric Mo clusters.

3.~~3~~ 2 Morphological and textural properties

Figure 56 reports some selected SEM micrographs: the main morphological difference between samples prepared by using ammonia or urea as precipitating agent is the particles size, as both C-MoCeZr-A and I-MoCeZr-A show smaller nanoparticles than the I-MoCeZr-U sample, where

sub-micrometer particles also occur. As XRD analysis evidenced differences in the crystalline phases occurring when two different precipitating agents were used, EXD mapping was adopted to figure out possible differences in the distribution of the three metals in the final products: the corresponding maps are reported in Fig. S4: with ammonia as precipitating agent, the Zr and Ce distribution in the EDX map revealed a fair mixing of the two elements, in agreement with the formation of a solid solution, whereas with urea, areas with higher Zr or Ce density were detected, in agreement with the previously discussed XRD results.

The Mo wt.% as measured by EDX analysis is reported in Table ~~5~~3: the two impregnated samples show a Mo content close to the nominal value, whereas lower Mo contents are obtained with the co-precipitated ones, probably due to incomplete precipitation of the Mo precursor.

Table ~~3~~5 also reports some textural data, as derived by the adsorption/desorption N_2 isotherms at -196 °C (Figure ~~6~~7): the samples have BET SSA values in the 66-95 $m^2\ g^{-1}$ range, ~~though~~ and the N_2 isotherms have different shape, depending on the precipitating agent. The NH_3 prepared samples show indeed type IV isotherms, with clear hysteresis loops evidencing the presence of a significant fraction of inter-particle mesoporosity, especially with the co-precipitated sample (C-MoCeZr-A) obtained by ~~the~~ a single step ~~method~~ (Fig. S5). On the other hand, the very limited hysteresis loops observed with urea-prepared samples suggest the main occurrence of narrow mesopores~~, mainly~~, *i.e.* of pores with diameter smaller than 3 nm, but still able to allow ~~the~~ diffusion of cyclooctene molecules (having a kinetic diameter of 0.55 nm [66]).

The values of Mo surface density, expressed as number of atoms per nm^2 surface area (Mo nm^{-2}) [52, 54], were calculated by dividing the Mo wt.% (as determined by EDX analysis) by the BET surface area. Such value may help evaluating the MoO_x dispersion degree, as the MoO_3 monolayer capacity on several metal oxide supports has been reported to be *ca*. 5 Mo nm^{-2} [55, 59-67, 68]. Below that value, only isolated and 2D-polymeric molybdate species are expected to form at the surface. The calculated Mo surface densities for the samples do not exceed the monolayer

capacity, being in the 3.3 – 5.3 range: however, the values obtained by the single step method are lower, indicating that a better Mo dispersion is obtained by co-precipitation.

3.43. Surface properties as studied by IR spectroscopy and NH_3 TPD.

Fig. 78 reports the IR spectra of the calcined (at 723 K) samples in the O–H stretching region (3800 – 3000 cm^{-1} range), as recorded after the vacuum pre-treatment, before NH_3 adsorption: all the IR spectra reported here were previously normalized to sample unit weight to allow comparison.

~~Fig. 8 reports the IR spectra of the calcined samples in the O–H stretching region (3800 – 3000 cm^{-1} range): all the IR spectra reported here were previously normalized to sample unit weight to allow comparison.~~

The IR spectrum of the C-CeZr-A support (Fig. 78a) shows an intense IR absorption due to a complex envelop of bands with at least three components centered at *ca*. 3756, 3670, 3510 cm^{-1} and a broad absorption towards lower wavenumbers, which is readily assigned to the occurrence of H-bonded OH groups. ~~In the~~According to the literature, the CeO_2 surface bears different types of hydroxyls, namely monodentate (Scheme 2), bidentate and tridentate species forming, when surface Ce^{4+} O^{2-} pairs dissociate water [69, 70]. The bands position is influenced by many factors, including the redox state of cerium, presence of surface vacancies and, here, also of Zr^{4+} ions. Indeed, hydroxyls at the surface of ZrO_2 have been found to absorb at *ca*. 3780-3770 cm^{-1} and 3680-3670 cm^{-1} [71, 72]. As a whole, the broadness and intensity of the OH stretching in Fig. 78a bands indicate that the support surface is highly defective and covered by a heterogeneous population of hydroxyls, finally hampering a straightforward assignment of all the bands.

However, impregnation mainly leads to the partial disappearance of the band centered at 3670 cm^{-1} (in the IR spectrum of I-MoCeZr-A), which could be mainly due to bidentate OH groups (type OH_{IIA}/OH_{IIB} in Scheme 2). The IR spectrum of the C-MoCeZr-A sample is, instead, very different, since also the band at *ca*. 3510 cm^{-1} is markedly affected by the presence of Mo species and, indeed,

Formattato: Colore carattere: Testo 1

Formattato: Colore carattere: Testo 1

Formattato: Colore carattere: Testo 1

decreases in intensity. The band at 3510 cm^{-1}, though very broad, indicates that it is likely due to heterogeneous tridentate OH species (OH_{III}): its disappearance in the co-precipitated sample indicates that Mo is likely occupying cation vacancies at the surface of the support in such a way that all the oxygen vacancies are occupied by the accompanying O anions, as already reported in the literature for Mo/CeO_2 systems obtained by heating mechanical mixtures of cerium nitrate and Mo oxide [56]. In the low wavenumbers range (1700 – 1150 cm^{-1}, not shown), the IR spectrum of the C-CeZr-A support shows several bands due to carbonate/bicarbonate species, which are almost totally suppressed upon impregnation and absent in the co-precipitated sample, confirming that the preparation procedure markedly affects also the surface properties, and not only the microstructure, of the catalysts.

Fig. 78b reports the IR spectra of the samples obtained by using urea, in the 3800 – 3000 cm^{-1} range: with respect to the C-CeZr-A ~~support,~~sample, the support obtained by using urea shows two additional components at about 3570 cm^{-1}, indicating the occurrence of a family of different OH species, and ~~-~~ at 3756 cm^{-1}, likely related to zirconia, as both XRD and Raman spectroscopy showed the occurrence of a separate phase. The IR spectra of the two catalysts prepared by using urea (Fig. 78b) resemble each other: with both catalysts, the bands at 3756 cm^{-1} disappears, indicating that Mo species are also interacting with the zirconia phase, in agreement with the XRD patterns, showing that the phase transition to *t*-ZrO_2 is hampered by the presence of Mo. Accordingly, with respect to the catalysts obtained by using ammonia, the band due to tri-dentate OH species is still ~~presence~~ present in both cases. In the low wavenumbers range (1700 – 1150 cm^{-1}, not shown), strong bands due to carbonate/bicarbonate species are observed in the IR spectrum of~~with~~ the support and not in the Mo-containing catalysts.

Fig. 78 shows that, independently of the precipitating agent, the presence of Mo is changing the surface of the samples and this fact should have an impact on their surface acid properties, which were studied by both NH_3 – TPD experiments and IR spectroscopy. The NH_3-TPD experiments (Fig. S6) evidenced different NH_3 adsorption capacity (tot mmol g^{-1}) among the studied samples: in

Formattato: Apice

particular, the overall amount of acid sites is higher (NH_3 ads. 0.15-0.18 mmol g^{-1}) with samples prepared by using ammonia with respect those prepared by using urea (0.05-0.11 mmol g^{-1}), indicating that the amount of acid sites is affected by the adopted procedure. Concerning the nature of Mo-related acid sites, however, the TPD profiles show that the addition of Mo promotes the formation of a new type of medium strength acid sites, besides those related to the support(s), independently of the precipitating agent used.

In order to figure out the nature of the Mo-related acid sites, NH_3 adsorption was followed by IR spectroscopy, the corresponding results on the four catalysts being summarized in Fig. 89 (and Fig. S7 for the supports).

In Figure 89, difference spectra are reported, as obtained after subtraction of the IR spectrum of the bare sample (Figure 78), concerning NH_3 ~~ammonia~~ adsorption (ca. 2000 Pa) and subsequent outgassing under vacuum at r.t. (curves 1) and at increasing temperatures (curves 2-4). By considering that, in difference spectra, positive bands concern species forming upon NH_3 ~~ammonia~~ adsorption, whereas negative bands concern surface species that interact with NH_3 ~~the ammonia~~ molecules, the curves in Fig. 89 show different bands: as a whole, NH_3~~ammonia~~ adsorption on the studied catalysts leads to the formation of both ammonium ions (by interaction with Brønsted acid sites, *i.e.* acidic –OH groups) and M^{x+}---NH_3 adducts (by interaction with Lewis acid sites, *i.e.* uncoordinated metal cations). The former species are responsible of the bands at *ca.* 1665 and 1480-1400 cm^{-1} (δ_{NH4+}), the latter of the bands at *ca.* 1600 cm^{-1} (δ_{asym} NH_3) and of the envelope in the 1250-1100 cm^{-1} range (δ_{sym} NH_3). Conversely, adsorption of NH_3~~ammonia~~ on both supports did not show the formation of ammonium species (Fig. S7), indicating that on those samples mainly Lewis acid sites are present, although those at the surface of the support prepared by using urea are slightly weaker, being removed at a lower outgassing temperature (*i.e.* 433 K instead of 513 K).

The position of the δ_{asym} NH_3 band of coordinated ammonia is sensitive to the acidic strength of the Lewis site, generally shifting towards higher wavenumbers as the acid strength increases [71, 73-74], and, thus, ~~so~~ the Lewis sites on the samples prepared by using ammonia seems stronger, as interaction

with NH_3~~ammonia~~ molecules leads to bands at 1601 cm^{-1} (C-MoCeZr-A) and 1604 cm^{-1} (I-MoCeZr-A), whereas the same band occurs at 1595 cm^{-1} and 1599 cm^{-1} with C-MoCeZr-U and I-MoCeZr-U, respectively. The stronger acidity of ~~the~~ Lewis sites obtained in the samples precipitated by ~~using~~ ammonia is confirmed by the fact that outgassing at 513 K does not lead to ~~the~~ complete desorption of the adsorbed species, which are instead totally desorbed in the samples prepared by using urea. This is also confirmed by inspection of the δ_{sym} NH_3, in that adsorption of NH_3 on the I-MoCeZr-A and C-MoCeZr-A catalysts leads to the formation of a pair of bands with maxima at 1222 and 1166 cm^{-1} and shoulders at 1218 and 1163 cm^{-1}, respectively, showing an opposite relative intensity of the two components. On the other hand, samples prepared using urea shows similar envelope of bands, with maximum at 1157 cm^{-1} (C-MoCeZr-U), and ill-defined shoulders at *ca*. 1114 and 1220 cm^{-1}. Comparison with IR spectra of the corresponding supports (Fig. S7) allows us assigning the 1218-1222 cm^{-1} component to NH_3 interacting with Mo species, and the lower wavenumbers component to NH_3 molecules interacting with the support.

This shows, indeed, that the choice of the precipitating agent affects the strength of the ~~resultant~~ resulting Lewis acid sites, in that the Lewis sites ~~occurring~~ at the surface of I-MoCeZr-A and C-MoCeZr-A are stronger. Nonetheless, the band at 1218-1222 cm^{-1} seems to be more stable ~~on~~ with the impregnated sample, which is, by the way more, active than the co-precipitated one, likely due to slightly more acid Lewis sites.

The different nature of the Lewis acid sites on the two set of catalysts is further evidenced by the negative band at *ca*. 1980 cm^{-1}, which is definitely more pronounced with the samples prepared using ammonia: as the IR spectra were normalized to sample unit ~~surface area~~weight, this means that species responsible of the negative band at *ca*. 1980 cm^{-1} are also more abundant in the samples prepared by using ammonia. In particular, such band is due to the first overtone of the Mo=O fundamental stretching mode (which falls at *ca*. 1000 cm^{-1}) of surface molybdenyl species [75, 76]. The consumption of the 1980 cm^{-1} band indicates that such molybdenyl species are coordinatively unsaturated, and may act as adsorption sites for NH_3~~ammonia~~ molecules, finally completing their

Formattato: Pedice

coordination sphere. Actually, previous studies showed that dispersion of molybdenum onto the surface of different metal oxides could lead both to ~~the strengthenin~~an increased acidity of the support ~~g of support~~ Lewis ~~acidity~~ sites and to the formation of new (moderately acidic) Lewis sites, involving Mo=O centers [71, 75, 76]. The different nature of the acid Lewis sites of the prepared samples was also evidenced by the different behavior of the adsorbed species upon thermal desorption under vacuum. In general, the decrease in intensity of $\delta_{sym}NH_3$ band is accompanied by a shift towards higher wavenumbers. With all the samples, the band is still detected after outgassing up to 433 K (curves 3), but only with sample C-MoCeZr-A the two components are stable up to 513 K, shifting from 1218 and 1166 cm^{-1} to 1248 and 1207 cm^{-1}, respectively. The relative intensity of the two components is almost preserved upon thermal desorption, suggesting a comparable acidity of the two families of sites. On the other hand, with sample I-MoCeZr-A, the two components shift from 1222 and 1163 cm^{-1} to 1245 and 1198 cm^{-1}, but the component at lower wavenumbers appears less stable upon thermal desorption, being consumed faster than the higher ~~frequency~~ wavenumbers one.

~~This~~ Such a different behavior could be explained by a ~~thorough~~ careful inspection of the Mo=O overtone mode, which is progressively restored (and shifted towards higher wavenumbers) upon NH_3~~ammonia~~ desorption (Fig. S7). Indeed, the corresponding negative band shows two distinct components at 1986 and 1974 cm^{-1} with sample C-MoCeZr-A, ~~while~~ whereas with sample I-MoCeZr-A it looks sharper, with a single component at 1982 cm^{-1}. This seem to indicate that the co-precipitation method favors the formation of two families of strong (Mo-based) Lewis sites, ~~while~~ whereas the impregnation leads to the formation of a family of stronger Mo-based sites, and a second one of (less strong) Me-based (Me = Ce or Zr) sites. This is in agreement with IR spectra in the OH stretching range (Fig. 7~~8~~a) showing that impregnation led to the consumption of mainly bidentate OH groups, whereas co-precipitation led ~~also~~ to the consumption of tri-dentate OH groups also. Finally, the new (weak) bands at 1637, 1561, 1456 and 1370 cm^{-1} ~~are~~ observed in the IR spectra of I-MoCeZr-A upon heating at 513 K can be assigned to species arising from NH_3~~ammonia~~ oxidation [77,78].

On the other hand, with the samples prepared using urea, similar changes in the $\delta_{sym}NH_3$ band are observed upon thermal desorption. The maximum of the peak~~s~~ shifts from 1157 to ca. 1177 cm^{-1}, whereas it is not possible to clearly identify a shift of the components at 1220 cm^{-1}, which seems to be still present after treatment at 433 K. In contrast, the shoulder at lower wavenumber (particularly evident with C-MoCeZr-U at ca. 1110 cm^{-1}) disappears almost completely after outgassing at 353 K. Finally, the intensity of the negative band due Mo=O species is very low as compared to that of $\delta_{sym}NH_3$ band, suggesting that ~~most~~ Lewis acidity is mainly due to coordinatively unsaturated Ce^{4+} and Zr^{4+} cations. The reason for such a difference in acidity between samples prepared with ammonia and urea was ~~unveiled~~ clarified by EDX mapping analysis of the samples (fig. S4) In fact, Figure-MAP clearly shows a homogeneous distribution of Ce, Zr, and Mo only ~~on~~ with the sample I-MoCeZr-A. In contrast, some particles agglomerates, where Ce is much more abundant than Zr and Mo, and some other regions where Zr and Mo are ~~the most~~more abundant ~~elements~~ are observed in the image of I-MoCeZr-U. This is in excellent agreement with XRD results, which evidenced only limited Zr dissolution into ceria fluorite lattice when urea is used as precipitating agent and confirms the tendency of Mo precursor to react preferentially with the amorphous ZrO_2, preventing its crystallization. Actually, also Raman ~~Spectroscopy~~ spectroscopy gave results in agreement ~~consistent~~ with this ~~interpretation~~hypothesis.

As far as Brønsted acidity is concerned, ~~the~~ addition of Mo to ~~different~~ other CeO_2, ZrO_2 and $Ce_xZr_yO_z$ systems was shown to promote the formation of Brønsted acid sites [73, 79-81]. ~~This~~ Such an effect is observed also with our catalysts, in particular with I-MoCeZr-A, which showed a large integrated absorption intensity of the ~~of~~ δ_{as} NH_4^+ band, even more intense than the Lewis-sites related bands. According to the literature, the relative strength of surface Brønsted and Lewis acid sites can be evaluated from the rate of decrease of the corresponding bands on heating, being expressed as (δ_{asym} NH_4^+) / (δ_{asym} NH_3) integrated absorbance ratio [71]. Such ratio was found to increase upon heating with all the samples studied here (*i.e.* Brønsted stronger than Lewis sites), ~~except with~~with

Formattato: Tipo di carattere: Non Corsivo

the exception of C-MoCeZr-A, where an almost constant value (*i.e.* a comparable strength for both types of sites) was obtained.

In the attempt of correlating the aforementioned acid surface properties of the samples with their catalytic activity (vide infra) ~~of the catalysts with the aforementioned acid surface properties~~, the following considerations may be drawn:

a) Independently on the adopted precipitating agent, Mo leads to the appearance of new Brønsted and Lewis sites. As a whole, the supports do not show Brønsted sites and have very weak Lewis sites.

b) ~~Catalysts~~ Samples prepared by using urea show a lower amount of Lewis sites with respect to those prepared by using ammonia.

c) In samples prepared by using ammonia, stronger Lewis sites form with respect to samples prepared by using urea. In particular, during co-precipitation two types of Lewis sites form, likely due to the reaction of bi-dentate and tri-dentated OH groups. The sample obtained by impregnation, however, shows slightly stronger acid Lewis sites related to Mo species.

3.~~1~~4 Catalytic tests

The epoxidation reaction of cyclooctene ~~was chosen for the activity study as it proceeds with the formation of corresponding epoxide without production of by-products, according to the reaction~~is reported in scheme 1.~~1.~~ Epoxycyclooctane is only product for this reaction [82~~38~~].

Fig. 9~~1~~ shows the profiles of cyclooctene conversion versus time for the Mo-containing catalysts reported in Table 1~~1~~ (the bare supports were not active)

High cyclooctene conversions were obtained in presence of the catalysts prepared by using ammonia, in that 94 % and 85 % conversion was reached after 24 h with I-MoCeZr-A and C-MoCeZr-A catalyst, respectively. Both catalysts obtained by using urea, regardless the type of synthesis method adopted (i.e. impregnation or co-precipitation), show a poor activity.

Formattato: Tabulazioni: Non a 6.5"

Formattato: Non Evidenziato

Formattato: Non Evidenziato

Moreover, much larger TOF (turn-over frequency) values (Table 42) were obtained when ammonia was used as the precipitating agent, with a large difference between I-MoCeZr-A and C-MoCeZr-A. Such different catalytic results have to be ascribed to markedly different ~~physico~~physic-chemical properties (*vide infra*).

The turn-over frequency per mol of molybdenum has been calculated as the cyclooctene consumption rate referred to the mole of molybdenum, eq. 1

$$TOF = \frac{1}{n_{Mo}} \frac{dn_{cycl.}}{\mathrm{dt}} \quad (1)$$

According to the literature, the oxidation reaction is promoted in presence of Lewis acid sites [83, 84~~39-40~~], and medium strength Lewis centres are commended as the most active in epoxidation [82~~38~~]. With this type of catalysts, the presence of Lewis acid sites is due to surface Mo species, in particular to isolated molybdenyl species that are depicted in literature as the most active Lewis acid sites in epoxidation [85-87~~41-43~~].

The measured TOF with I-MoCeZr-A is comparable to that reported by Arnold et al. [35~~28~~] for Mo/SiO_2 catalyst that, however, showed leaching issue (at 80 °C from fig. 2 of [35~~28~~] it is possible to calculate a TOF of about 0.34 s^{-1}). More recently, Shen et al. [13] reviewed the progress of molybdenum-based catalysts and the TOF reported for oxides (SiO_2, ZrO_2, TiO_2) supported molybdenum active species are lower with respect to ones of I-MoCeZr-A and C-MoCeZr-A.

In this work, the possible leaching of active species into the liquid phase under operating conditions was verified according the method reported by Sheldon [51~~44~~], *i.e.* by removing the catalyst from the reaction mixture by filtration after 150 min from the start of the reaction, and by deter mining the residual conversion for additional 150 min. The tests were perform~~inged~~ on the two most active catalysts (I-MoCeZr-A and C-MoCeZr-A) and ~~For each catalyst,~~ almost no cyclooctene conversion in the filtrate was detected after the catalyst removal, providing a very strong evidence that such materials act as real heterogeneous catalysts. For the catalyst I-MoCeZr-A, the leaching test was also conducted for 24 hours ,after removing the catalyst ~~removing for 24 hours~~ without significa~~tivent~~

Formattato: Non Evidenziato

changes in the conversion of cyclooctene. Moreover, the almost total absence of Mo leaching was confirmed by ICP spectroscopic analysis carried out on the reaction solution, where a concentration of Mo less than 30 ppm was detected.

From the point of view of possible industrial applications, catalyst stability is a crucial issue and, therefore, with the most active, catalysts stability was assessed by performing three runs, as follows: after each run, the solid was separated by filtration and directly reused for a new run, without washing, the corresponding results being reported in Table 53. Again, any possible leaching phenomenon was excluded by ICP analysis of the reaction solution.

With both the catalysts, the activity loss can be considered limited, as no washing was performed: such phenomenon can indicate that the catalysts are quite stable and are comparable to other catalysts obtained by more complicated synthesis and where chlorinated solvent were used in the reaction [13]. As a whole, both the I-MoCeZr-A and C-MoCeZr-A samples behave as true heterogeneous catalysts, with no leaching and good stability. The observed reduction in final conversion could be due to the blocking of catalytic sites by fouling [3528], as the powders were not pre-treated (solvent washing or calcination) before each reuse cycle.

c)

Formattato: Non Evidenziato

Formattato: Inglese (Regno Unito)

Formattato: Nessun elenco puntato o numerato

Conclusions

Excellent catalytic performances in the epoxidation of cyclooctene with cumene hydroperoxide are obtained in the presence of ceria-zirconia supported molybdenum oxide. Still moreMoreover, the catalysts are stable and behaves as actual heterogeneous catalysts. Nevertheless, the catalytic behaviour strongly depends strongly on the synthesis route and, in particular, on the precipitating agent.

The physico-chemical characterization showed that s.

Small oligomeric MoOx clusters were successfully dispersed onto a solid solution $Ce_{0.75}Zr_{0.25}$ exclusively by using ammonia as precipitating agent, by either coprecipitation or impregnation

method. X-ray Diffraction and Raman spectroscopy revealed a ~~marked~~ clear phase separation with ~~the~~ formation of cerianite and tetragonal zirconia in the samples prepared by using urea as precipitating agent.

Concerning surface properties, b~~B~~oth Brønsted and Lewis sites were detected in all the Mo-containing samples, whereas the supports do not show Brønsted sites and only~~have~~ very weak Lewis sites.

The presence of larger amount of Mo-related Lewis acid sites in the samples prepared by using ammonia is the crucial feature ~~shown by samples prepared using ammonia~~ affecting their catalytic activity in the cyclooctene epoxidation reaction. ~~This~~ Such a finding ~~conclusion seems to be~~is in agreement with previous studies, which ~~evidence~~ pointed out the ~~importance of~~ positive effect of the catalytic activity towards cyclooctene epoxidation of mildly acidic surface sites.~~a moderate strength acidity in the catalytic activity of this reaction~~.

References

1. G. Sienel, R. Rieth, K.T. Rowbottom, Epoxides, in: Ullmann (ed.), Ullmann's Encyclopedia of Industrial Chemistry, Wiley-VCH, Weinheim, 2000, pp139-152.
2. K. Bauer, D. Garbe, H. Surburg, Common Fragrance and Flavour Materials, fourth ed., Wiley-VCH, Weinheim, 2001.
3. A.K. Yudin, Aziridines and Epoxides in Organic Synthesis, first ed., Wiley-VCH, Weinheim, 2006.
4. K. Ambroziak, R. Mbeleck, B. Saha, D.C.J. Sherrinton, Ion exchange 18 (2007) 598-603.
5. K. Ambroziak, R. Mbeleck, Y. He, B. Saha, D.C. Sherrington, Ind. Eng. Chem. Res. 48 (2009) 3293-3302.
6. K. Ambroziak, R. Mbeleck, B. Saha, D.C. Sherrington, Int. J. Chem. React. Eng. 8 (2010) 1-13.
7. R. Mbeleck, K. Ambroziak, B. Saha, D.C. Sherrington, React. Funct. Polym. 67 (2007) 1448-1457.
8. M.L. Mohammed, R. Mbeleck, D. Patel, D. Niyogi, D.C. Sherrington B. Saha, Chem. Eng. Res. Des. 94 (2015) 194-203.
9. H. Shi, Z. Zhang, Y. Wang, J. Mol. Catal. A: Chem. 238 (2005) 13-25
10. E. Santacesaria, V. Russo, R. Tesser, R. Turco, M. Di Serio, Ind. Eng. Chem. Res 56 (2017) 12940-12952.
11. R. Turco, C. Pischetola, M. Di Serio, R. Vitiello, R. Tesser, E. Santacesaria, Ind. Eng. Chem. Res. 56 (2017) 7930-7936.
12. G. Grigoropoulou, J.H. Clark, J.A. Elings, Green Chemistry 5 (2003) 1–7.
13. Y. Shen, P. Jiang, P. Thin Wai, Q. Gu, W. Zhang, Catalysts 9 (2019) 31.
14. X. Liu, J. Ding, X. Lin, R. Gao, Z. Li, W.L. Daia, Appl. Catal. A: Gen. 503 (2015) 117–123.
15. B. Singh, B.S. Rana, L.N. Sivakumar, G.M. Bahuguna, A.K. Sinha, J. Porous Mat. 20 (2013) 397-405.

16. J.L. Zheng, J. Warna, T. Salmi, F. Burel, B. Taouk, S. Leveneur, AIChE J. 65 (2016) 726-741.

17. M. Di Serio, V. Russo, E. Santacesaria, R. Tesser, R. Turco, R. Vitiello, Ind. Eng. Chem. Res. 56 (2017) 12963-12971.

18. B. Notari, Cataysis Today 18 (1993) 163-172.

19. S.T. Oyama, Mechanism in homogeneous and heterogeneous epoxidation catalysis, first ed., Elsevier Science, Amsterdam, 2008.

20. M. Herbert, A. Galindo, F. Montilla, Catal. Comm. 8 (2007) 987-990.

21. A.M. Martins, C.C. Romão, M. Abrantes, M.C. Azevedo, J. Cui, A.R. Dias, M.T. Duarte, M.A. Lemos, T. Lourenço, R. Poli, Organometallics 24 (11) (2005) 2582–2589.

22. R.J. Cross, P.D. Newman, R.D. Peacock, D. Stirling, J. Mol. Catal. A: Chem. 144 (1999) 273–284.

23. A.A. Valente, J. Moreira, A.D. Lopes, M. Pillinger, C.D. Nunes, C.C. Romão, F.E. Kühn, I.S. Gonçalves, New J. Chem.28 (2004) 308-313.

24. J.M. Mitchell, Nathaniel S. Finney, J. Am. Chem. Soc. 123 (2001) 862-869.

~~22.~~25. M. Abrantes, T.R. Amarante, M.M. Antunes, S. Gago, F.A. Almeida Paz, I. Margiolaki, A.E. Rodrigues, M. Pillinger, A.A. Valente, I.S. Gonçalves, Inorg. Chem. 49 (2010) 6865–6873.

~~23.~~26. S. Shylesh, M. Jia, W.R. Thiel, Eur. J. Inorg. Chem. (2010) 4395 − 4410.

~~24.~~27. J. Moreno, J. Iglesias, J.A. Melero, Catalysts 7 (2017) 215.

28. F. Bigi, C.G. Piscopo, G. Predieri, G. Sartori, R. Scotti, R. Zanoni, R. Maggi, J. Mol. Catal. A: Chem. 386 (2014) 108–113.

29. P. Ferreira, I.S. Gonçalves, F.E. Kühn, M. Pillinger, J. Rocha, A. Thursfield, W.M. Xue, G. Zhang, J. Mater. Chem.10 (2000) 1395-1401.

Formattato: Italiano (Italia)

Formattato: Italiano (Italia)

Codice campo modificato

Formattato: Inglese (Regno Unito)

Formattato: Inglese (Regno Unito)

Formattato: Inglese (Regno Unito)

Formattato: Inglese (Regno Unito)

Codice campo modificato

Codice campo modificato

Codice campo modificato

Formattato: Inglese (Regno Unito)

Formattato: Inglese (Regno Unito)

Codice campo modificato

Codice campo modificato

30. M. V. Dias, M.S. Saraiva, P. Ferreira, M. J. Calhorda, Organometallics 34 (2015) 1465 − 1478.

~~25.~~31. M. Jia, A. Seifert, W.R. Thiel, Chem. Mater. 15 (2003) 2174-2180.

32. J.H. Ahn, J.C. Kim, S.K. Ihm, C.G. Oh, D.C. Sherrington, Ind. Eng. Chem. Res. 44 (2005) 8560-8564.

~~26.~~33. Y. Kuwahara, N. Furuichi, H. Seki H. Yamashita, J. Mater. Chem. A 5 (2017) 18518-18526.

~~27.~~34. G. Grivani, S. Tangestaninejad, M.H. Habibi, V. Mirkhani, M. Moghadam, Appl. Catal. A: Gen. 299 (2006) 131–136.

~~28.~~35. U. Arnold, R.S. Da Cruz, R.D. Mandelli, U. Schuchardt, J. Mol. Catal. A: Chem. 165 (2001) 149–158.

~~29.~~36. M. Shokouhimehr, Y. Piao, J. Kim, Y. Jang, T. Hyeon, Angew. Chem. Int. Ed. 46 (2007) 7039 –7043.

~~30.~~37. P. Chandra, D.S. Doke, S.B. Umbarkarab, A.V. Biradar, J. Mater. Chem. A 2 (2014) 19060–19066.

~~31.~~38. H. Noh, Y. Cui, A.W. Peters, D.R. Pahls, M.A. Ortuño, N.A. Vermeulen, C.J. Cramer, L. Gagliardi, J.T. Hupp, O.K. Farha, J. Am. Chem. Soc. 138 (2016) 14720 − 14726.

~~32.~~39. G. Dell'Agli, G. Mascolo, M.C. Mascolo, C. Pagliuca, J. Amer. Ceram. Soc. 91 (2008) 3375-3379.

~~33.~~40. G. Accardo, L. Spiridigliozzi, R. Cioffi, C. Ferone, E. Di Bartolomeo, S.P. Yoon, G. Dell'Agli, Mat Chem Phys 187 (2017) 149-155.

~~34.~~41. L. Spiridigliozzi, G. Dell'Agli, A. Marocco, G. Accardo, M. Pansini, Y. Kwon, S.P. Yoon, D. Frattini, J. Ind Eng Chem 59 (2018) 17-27.

~~35.~~42. S. Esposito, M. Turco, G. Bagnasco, C. Cammarano, P. Pernice, Appl. Catal. A: Gen. 403 (2011) 128–135.

~~36.~~43. L. Spiridigliozzi, G. Dell'Agli, M. Biesuz, V. Sglavo, M. Pansini, Adv Mat. Sci. Eng. 2016 Article ID 6096123, 8 pages.

~~37.~~44. T.J.B. Holland, S.A.T. Redfern, Mineral. Mag. 61 (1997) 65-77.

~~38. M. Cozzolino, M. Di Serio, R. Tesser, E. Santacesaria, Appl. Catal. A: Gen. 325 (2007) 256–262.~~

~~39. M.G. Finn, K.B. Sharpless, J. Am. Chem. Soc. 113(1) (1991) 113-126.~~

~~40. P. Iengo, G. Aprile, M. Di Serio, D. Gazzoli, E. Santacesaria, Appl. Catal. A: Gen. 178 (1999) 97-109.~~

~~41. A. Corma, H. García, Chem. Rev. 102 (2002) 3837-3892.~~

~~42. I. Rossetti, G.F. Mancini, P. Ghigna, M. Scavini, M. Piumetti, B. Bonelli, F. Cavani, A. Comite, J. Phys. Chem. C 116 (2012) 22386-22398.~~

~~43. I. Rossetti, L. Fabbrini, N. Ballarini, C. Oliva, F. Cavani, A. Cericola, B. Bonelli, M. Piumetti, E. Garrone, H. Dyrbeck, E.A. Blekkan, L. Forni, J. Catal. 256 (2008) 45-61.~~

~~44. I.W.C.E. Arends, R.A. Sheldon, Appl. Catal. A: Gen. 212 (2001) 175–187.~~

45. M. Biesuz, G. Dell'Agli, L. Spiridigliozzi, C. Ferone, V. Sglavo, Ceram. Int. 42 (2016) 11766-11771.

46. S.J. Costenoble, I. Rumaux, E. Odore, S. Picart, J. Nucl. Sci Tech. 55 (2018) 1235-1244.

47. G. Dell'Agli, G. Mascolo, M.C. Mascolo, C. Pagliuca, Solid State Sci 8 (2006) 1046-1050.

48. T. Tsoncheva, R. Ivanova, J. Henych, M. Dimitrov, M. Kormunda, D. Kovacheva, N. Scotti, V. Dal Santo, V. Štengl, Appl. Catal. A: Gen. 502 (2015) 418–432.

49. S.A. Acharya, V.M. Gaikwad, V. Sathe, S.K. Kulkarni, Appl. Phys. Lett. 104 (2014) 113508.

50. L. Li, F. Chen, J.Q. Lu, M.F. Luo, J. Phys. Chem A 115 (2011), 7972-7977.

51. C. Andriopoulou, A. Trimpalis, K.C. Petallidou, A. Sgoura, A.M. Efstathiou, S. Boghosian, J. Phys. Chem. C 121 (2017) 7931-7943.

52. S. Xie, K. Chen, A.T. Bell, E. Iglesia, J. Phys. Chem. B 104 (2000) 10059-10068.

Codice campo modificato

Codice campo modificato

53. F. Zhang, C.H. Chen, J. Am. Ceram. Soc. 89 (2006) 1028–1036.

54. G. Tsilomelekis, A. Christodoulakis, S. Boghosian, Catal. Today 127 (2007) 139–147.

55. P. Dufresne, E. Payen, J. Grimblot, J.P. Bonnelle, J. Phys. Chem. 85 (1981) 2344-2351.

56. X. Du, L. Dong, C. Li, Y. Liang, Y. Chen, Langmuir 15 (1999) 1693-1697.

57. Y. Peng, R. Qu, X. Zhang, J. Li, Chem. Comm. 49 (2013) 6215-6217.

58. H. Wan, D. Li, H. Zhu, Y. Zhang, L. Dong, Y. Hu, B. Liu, K. Sun, L. Dong, Y. Chen, J Colloid Interf. Sci. 326 (2008) 28-34.

59. F. Prinetto, G. Cerrato, G. Ghiotti, A. Chiorino, J. Phys. Chem. 99 (1995) 5556-5567.

60. B. Samaranch, P.R. de la Piscina, G. Clet, M. Houalla, N. Homs, Chem. Mater.18 (2006) 1581-1586.

61. K. Chen, S. Xie, E. Iglesia, A.T. Bell, J. Catal. 189 (2000) 421-430.

62. K.Y.S. Ng, E. Gulari, J. Catal. 92 (1985) 340-354.

63. A.H. Zapién, J.M.H. Enríquez, R.G. Alamilla, G.S. Robles, U.P García, L.A.G. Serrano, Adv. Mat. Sci. Eng. 8 (2014) ID 432031.

64. M. Valigi, A. Cimino, D. Cordischi, S. De Rossi, C. Ferrari, G. Ferraris, D. Gazzoli, V. Indovina, M. Occhiuzzi, Solid States lonics 63-65 (1993) 136-142.

65. R. Si, Y.W. Zhang, S.J. Li, B.X. Lin, C.H. Yan, J. Phys. Chem. B 108 (2004) 12481-12488.

66. C.J. Stephenson, J.T. Hupp, O.K. Farha, Inorg. Chem. Front. 2 (2015) 448 – 452.

67. Y. Xie, Y. Tang, Adv. Catal. 37 (1990) 1-43.

68. J. Edwards, R.D. Adams, P.D. Ellis, J. Am. Chem. Soc. 112 (1990) 8349 – 8364.

69. C. Binet, M. Daturi, J.C. Lavalley, Catal Today 50 (1999) 207-225.

70. T.R. Sahoo, M. Armandi, R. Arletti, M. Piumetti, S. Bensaid, M. Manzoli, S.R. Panda, B. Bonelli, Appl. Catal. B: Environmental, 211 (2017), 31-45.

71. G. Ramis, L. Yi, G. Busca, M. del Arco, C. Martìn, V. Rives, V. Sanchez Escribano, Mater. Chem. Phys. 55 (1998) 173-187.

72. G. Cerrato, S. Bordiga, S. Barbera, C. Morterra, Surf. Sci. 377-379 (1997) 50-55.

73. A.A. Tsyganenko, D.V. Pozdnyakov, V.N. Filimonov, J. Mol. Struct. 29 (1975) 299-318.

74. L. Dall'Acqua, I. Nova, L. Lietti, G. Ramis, G. Busca, E. Giamello, Phys. Chem. Chem. Phys. 2 (2000) 4991-4998.

75. M. Del Arco, C. Martìn, V. Rives, V. Sanchez Escribano, G. Ramis, G. Busca, V. Lorenzelli, P. Malet, J. Chem. Soc., Faraday Trans., 89 (1993) 1071-1078.

76. S. Payen, S. Kasztelan, J. Grimblot, J.P. Bonnelle, J. Raman Spectrosc.17 (1986) 233-241.

77. G. Ramis, L. Yi, G. Busca, M. Turco, E. Kotur, R.J. Willey, J. Catal. 157 (1995) 523-535.

78. L. Zhang, J. Pierce, V. L. Leung, D. Wang, W.S. Epling, J. Phys. Chem. C 117 (2013) 8282−8289.

79. Z. Liu, H. Su, J. Li, Y. Li, Catal. Comm. 5 (2015) 51-54.

80. X. Li, Y. Li, Catal. Lett. 144 (2014) 165–171.

81. M. Wang, Z. Si, L. Chen, X. Wu, J. Yu, Rare Earth, 31 (2013) 1148-1156.

82. M. Cozzolino, M. Di Serio, R. Tesser, E. Santacesaria, Appl. Catal. A: Gen. 325 (2007) 256–262.

83. M.G. Finn, K.B. Sharpless, J. Am. Chem. Soc. 113(1) (1991) 113-126.

84. P. Iengo, G. Aprile, M. Di Serio, D. Gazzoli, E. Santacesaria, Appl. Catal. A: Gen. 178 (1999) 97-109.

85. A. Corma, H. García, Chem. Rev. 102 (2002) 3837-3892.

86. I. Rossetti, G.F. Mancini, P. Ghigna, M. Scavini, M. Piumetti, B. Bonelli, F. Cavani, A. Comite, J. Phys. Chem. C 116 (2012) 22386-22398.

87. I. Rossetti, L. Fabbrini, N. Ballarini, C. Oliva, F. Cavani, A. Cericola, B. Bonelli, M. Piumetti, E. Garrone, H. Dyrbeck, E.A. Blekkan, L. Forni, J. Catal. 256 (2008) 45-61.

88. I.W.C.E. Arends, R.A. Sheldon, Appl. Catal. A: Gen. 212 (2001) 175–187.

Captions to Figures

Scheme 1 Reaction pathway

Scheme 2 Types of OH species found at the surface of CeO_2 according to the literature [70]

~~**Figure 1** Cyclooctene conversion vs time profiles in presence of Mo-containing catalysts. Reaction conditions: 300 mg catalyst; 9.78 g cyclooctene; 24.5 g of a solution containing 80 wt. % of cumene hydroperoxide; T =80°C.~~

Figure 12 XRD patterns of the catalysts and the relative support prepared by using ammonia. (* tetragonal zirconia, ICDD card No. 50-1089).

Figure 23 Raman spectra of the catalysts and the relative support prepared by using ammonia. Inset: magnification of the most intense band.

Figure 34 XRD patterns of the catalysts and the relative support prepared by using urea. (* tetragonal zirconia, ICDD card No. 50-1089. o cerianite, CeO_2, ICDD card. No. 34-394)

Figure 45 Raman spectra of the catalysts and the relative support prepared by using urea.

Figure 56 FESEM micrographs of C-MoCeZr-A (**a),** I-MoCeZr-A (**b**) and I-MoCeZr-U (**c**).

Figure 67. N_2 adsorption/desorption isotherms at 196 °C of I-MoCeZr-A (circles), C-MoCeZr-A (diamonds), I-MoCeZr-U (triangles), and C-MoCeZr-U (stars).

Figure 7~~8~~ OH region of the IR spectra of pre-treated samples, prepared using ammonia (section a) and urea (section b).

Figure 8~~9~~ Difference FTIR spectra of the adsorbed species arising from ammonia adsorption and subsequent outgassing at r.t. (curves 1), 353 K (curves 2), 433 K (curves 3), 513 K (curves 4).

Figure 9~~1~~ Cyclooctene conversion vs time profiles in presence of Mo-containing catalysts. Reaction conditions: 300 mg catalyst; 9.78 g cyclooctene; 24.5 g of a solution containing 80 wt. % of cumene hydroperoxide; T =80°C.

Table 1 List of all the as-synthesized ceria zirconia supported molybdenum samples, along with their samples code and synthesis conditions.

Label	Sample	Mo-addition method	Synthesis temperature, °C
C-CeZr-A	$Zr_{0.25}Ce_{0.75}O_2$	Co-precipitation (ammonia)	r.t.
C-MoCeZr-A	MoO_x- $Ce_{0.75}Zr_{0.25}O_2$	Co-precipitation (ammonia)	90
I-MoCeZr-A	$MoO_x/Ce_{0.75}Zr_{0.25}O_2$	Wet-impregnation (ammonia)	r.t.
C-CeZr-U	$Ce_{0.75}Zr_{0.25}O_2$	Co-precipitation (urea)	90
C-MoCeZr-U	MoO_x- $Ce_{0.75}Zr_{0.25}O_2$	Co-precipitation (urea)	90
I-MoCeZr-U	$MoO_x/Ce_{0.75}Zr_{0.25}O_2$	Wet -impregnation (urea)	90

~~**Table 2** TOF values calculated for the runs reported in Figure 1, by considering the actual Mo contents as reported in Table 5. Reaction conditions: 300 mg catalyst, 9.78 g cyclooctene, 24.5 g of a solution containing 80 wt% of cumene hydroperoxide; T = 80°C~~

~~Sample~~	~~TOF (s^{-1})~~
~~I-MoCeZr-A~~	~~1.16E-1~~

~~C-MoCeZr-A~~	~~6.90E-2~~
~~I-MoCeZr-U~~	~~4.11E-3~~
~~C-MoCeZr-U~~	~~4.18E-3~~

~~**Table 3** Cyclooctene conversion (5) as obtained during the stability tests. Reaction conditions. 300 mg of catalyst at 1st cycle; for each runs 9.78 g of cyclooctene, 24.5 g of a solution containing 80 wt. % of cumene hydroperoxide; T = 80°C~~

~~Catalyst~~	~~Cycle~~	~~Conversion (%)~~
~~C-MoCeZr-A~~	~~1st~~	~~71.0~~
	~~2nd~~	~~70.3~~
	~~3rd~~	~~65.8~~
~~I-MoCeZr-A~~	~~1st~~	~~80.0~~
	~~2nd~~	~~76.6~~
	~~3rd~~	~~65.6~~

Table 24 Lattice parameter and crystallite size of the various samples

Sample	***a* (nm)**	***d_{cryst} (nm)***
C-MoCeZr-A	0.5403±1.5E–4	7.7
C-MoCeZr-U	0.5423±2.0E–4	10.9
I-MoCeZr-U	0.5410±1.6E–4	11.0
I-MoCeZr-A	0.5391±4.6E–4	8.2

C-CeZr-A	0.5396±2.9E–4

CeO_2 a = 0.5411 nm (ICDD card No. 34-394); $Ce_{0.75}Zr_{0.25}$ a = 0.5349 nm (ICDD card No. 28-271).

Table 35. Composition and textural data of the prepared samples

Sample	S.S.A. (m^2g^{-1})	Total Pore volume (cm^3g^{-1})	Mo wt.% (EDX)	Mo surface density (Mo atoms nm^{-2})
C-CeZr-A	76	6.9E-2	-	-
I-MoCeZr-A	84	8.3E-2	7.1	5.3
C-MoCeZr-A	94	1.4E-1	6.1	4.1
C-CeZr-U	66	6.0E-2	-	-
I-MoCeZr-U	90	6.8E-2	6.4	4.4
C-MoCeZr-U	95	8.4E-2	5.3	3.3

Table 4 TOF values calculated for the runs reported in Figure 9, by considering the actual Mo contents as reported in Table 3. Reaction conditions: 300 mg catalyst, 9.78 g cyclooctene, 24.5 g of a solution containing 80 wt% of cumene hydroperoxide; T = 80°C

Sample	TOF (s^{-1})
I-MoCeZr-A	1.16E-1
C-MoCeZr-A	6.90E-2

I-MoCeZr-U	4.11E-3
C-MoCeZr-U	4.18E-3

Table 5 Cyclooctene conversion (5) as obtained during the stability tests. Reaction conditions. 300 mg of catalyst at 1st cycle; for each runs 9.78 g of cyclooctene, 24.5 g of a solution containing 80 wt. % of cumene hydroperoxide; T = 80°C

Catalyst	Cycle	Conversion (%)
C-MoCeZr-A	1st	71.0
	2nd	70.3
	3rd	65.8
I-MoCeZr-A	1st	80.0
	2nd	76.6
	3rd	65.6

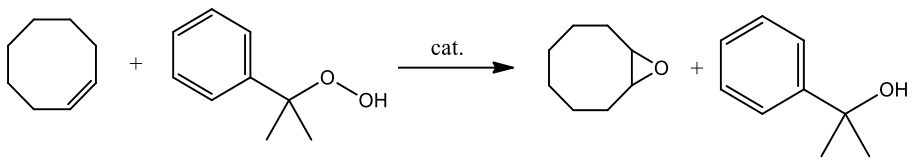

Scheme 1

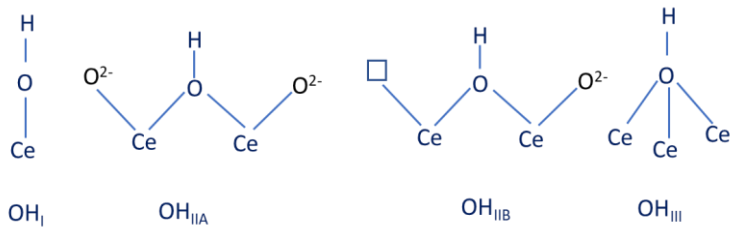

Scheme 2

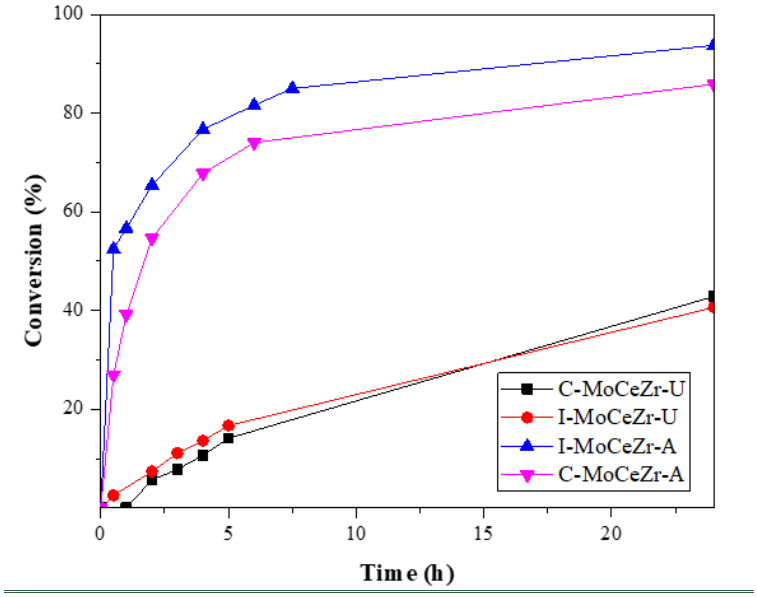

~~Figure 1~~

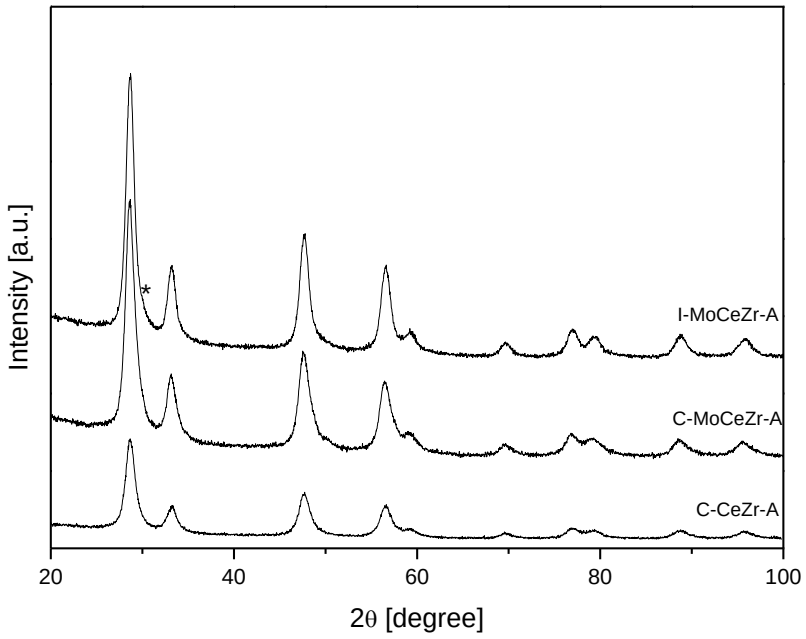
Intensity [a.u.]
*
I-MoCeZr-A
C-MoCeZr-A
C-CeZr-A
20
40
60
80
100
2θ [degree]

Figure 12

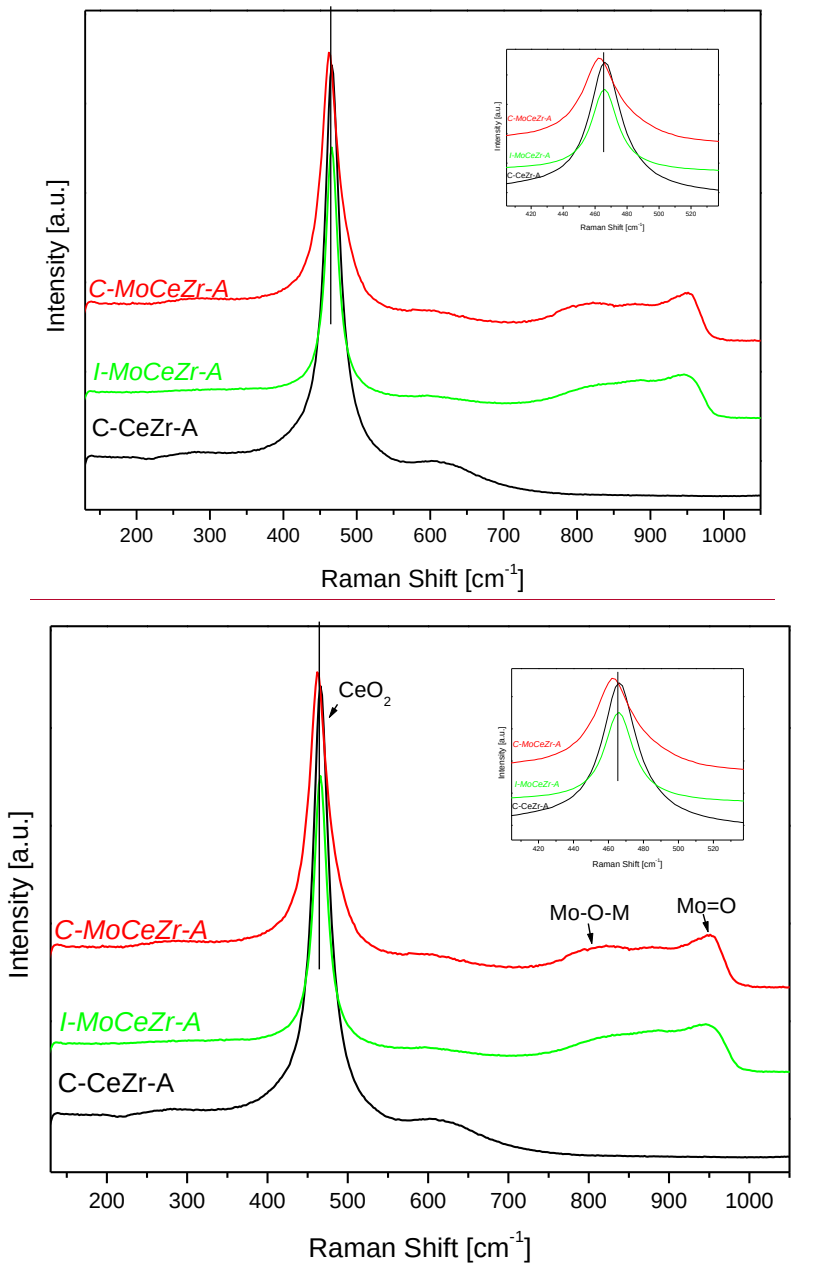
Intensity [a.u.]
C-MoCeZr-A
I-MoCeZr-A
C-CeZr-A
200
300
400
500
600
700
800
900
1000
Raman Shift [cm-1]
CeO2
Mo-O-M
Mo=O

Figure 23

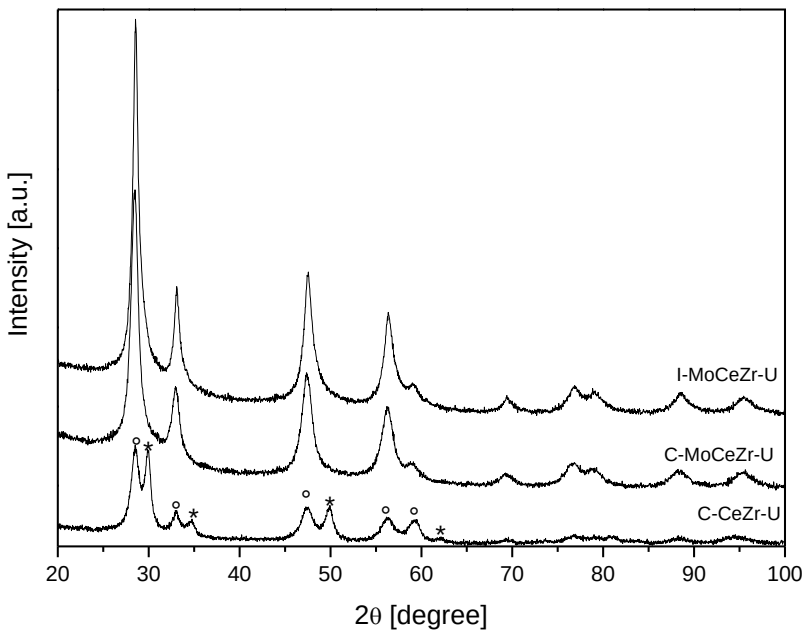
Intensity [a.u.]
I-MoCeZr-U
C-MoCeZr-U
C-CeZr-U
20
30
40
50
60
70
80
90
100
2θ [degree]

Figure 34

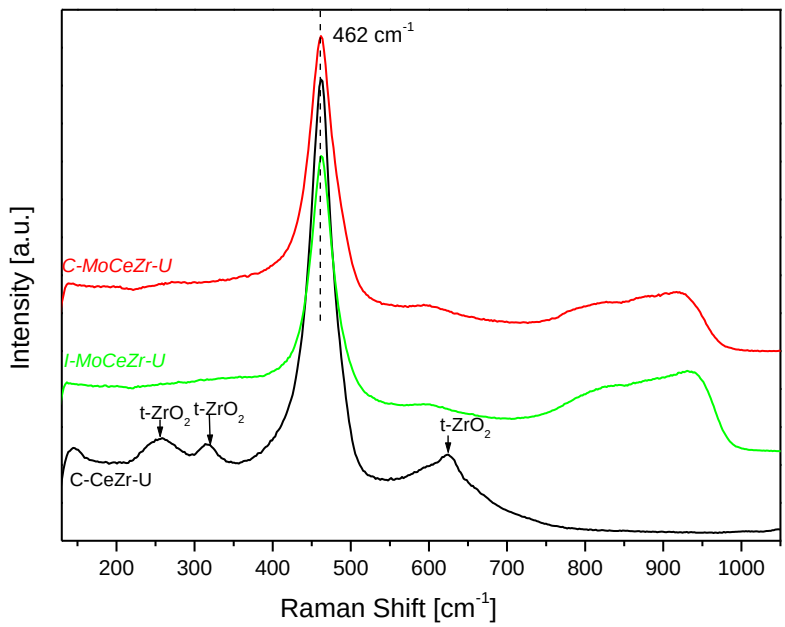
462 cm-1
C-MoCeZr-U
I-MoCeZr-U
t-ZrO2
t-ZrO2
t-ZrO2
C-CeZr-U
Intensity [a.u.]
200
300
400
500
600
700
800
900
1000
Raman Shift [cm-1]

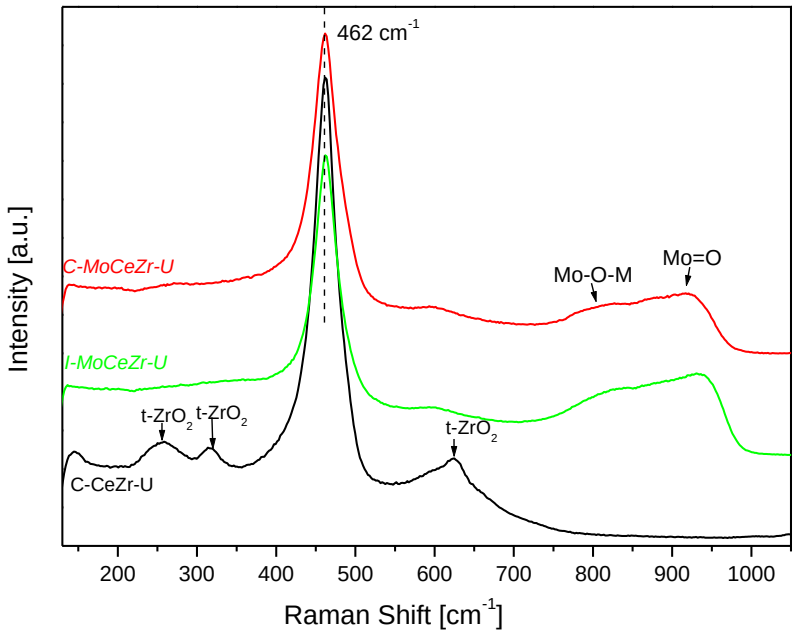
462 cm-1
C-MoCeZr-U
I-MoCeZr-U
C-CeZr-U
Mo-O-M
Mo=O
t-ZrO2
t-ZrO2
t-ZrO2
Intensity [a.u.]
200
300
400
500
600
700
800
900
1000
Raman Shift [cm-1]

Figure 45

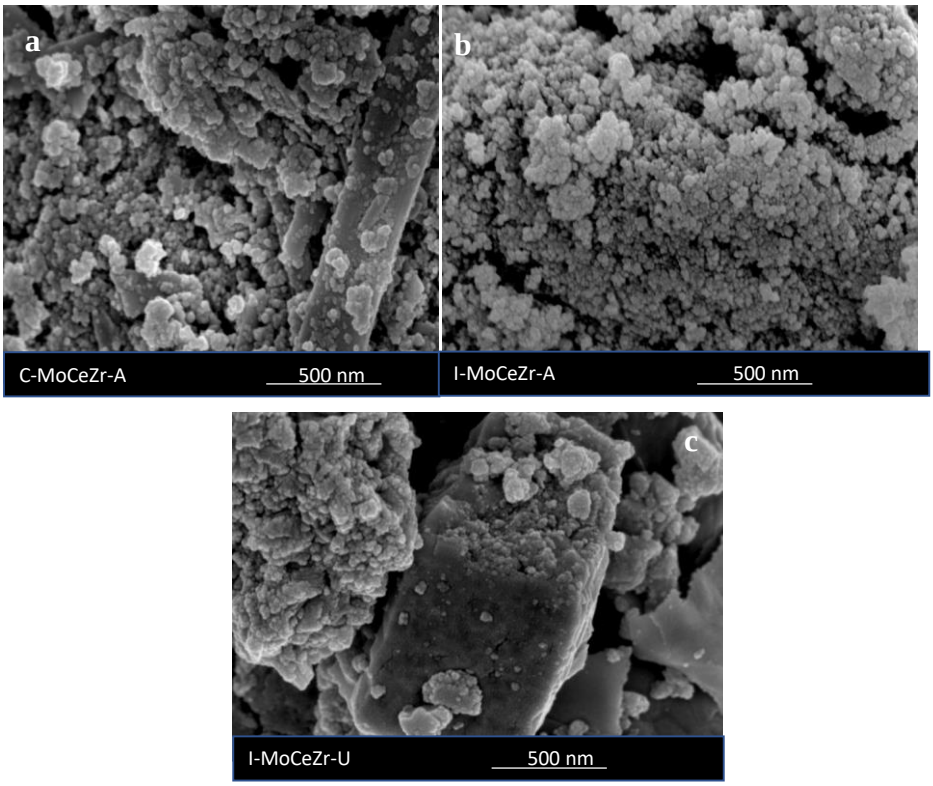

Figure 56

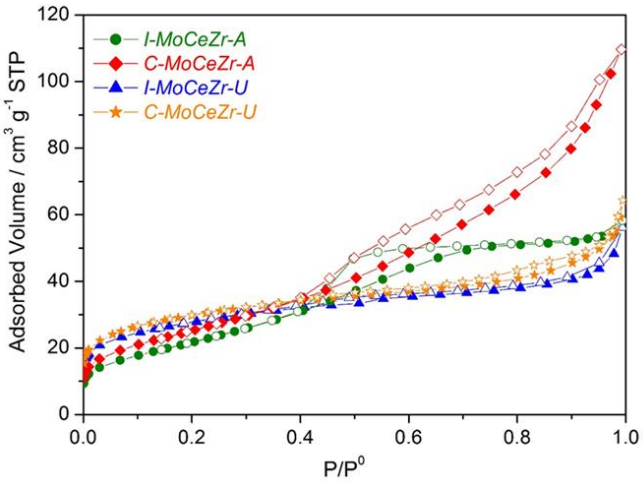
I-MoCeZr-A
C-MoCeZr-A
I-MoCeZr-U
C-MoCeZr-U
Adsorbed Volume / cm3 g-1 STP
P/P0
0
20
40
60
80
100
120
0.0
0.2
0.4
0.6
0.8
1.0

Figure 67

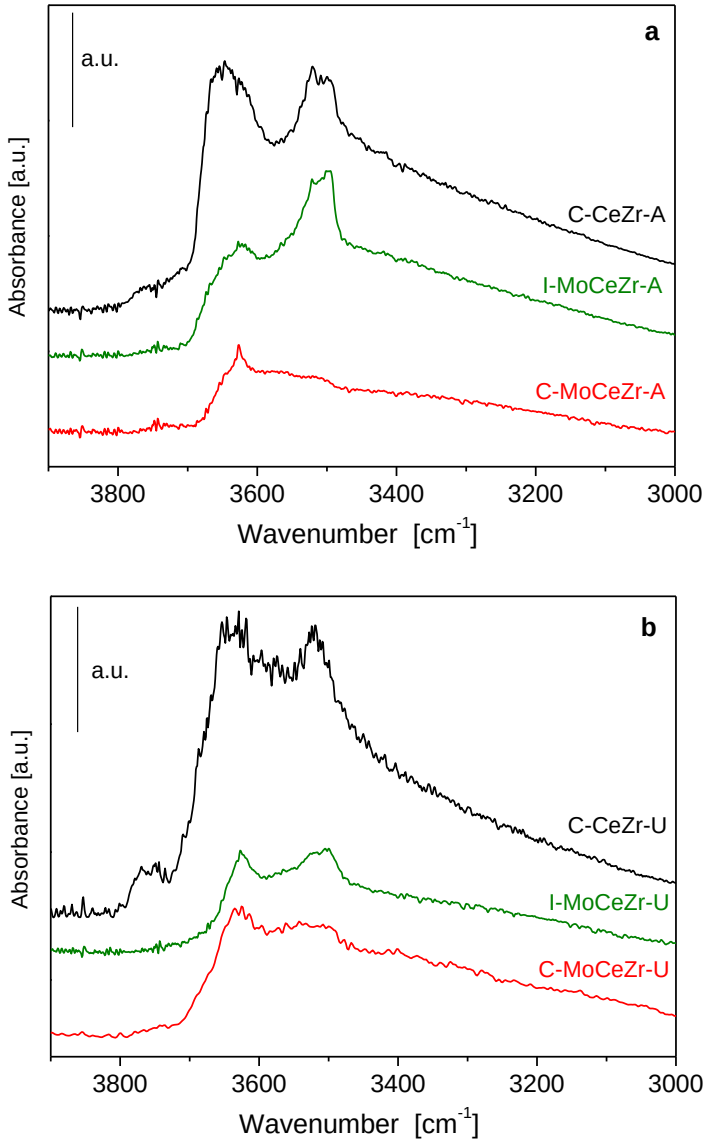
a
a.u.
C-CeZr-A
I-MoCeZr-A
C-MoCeZr-A
Absorbance [a.u.]
3800
3600
3400
3200
3000
Wavenumber [cm-1]
b
a.u.
C-CeZr-U
I-MoCeZr-U
C-MoCeZr-U
Absorbance [a.u.]
3800
3600
3400
3200
3000
Wavenumber [cm-1]

Figure 7~~8~~

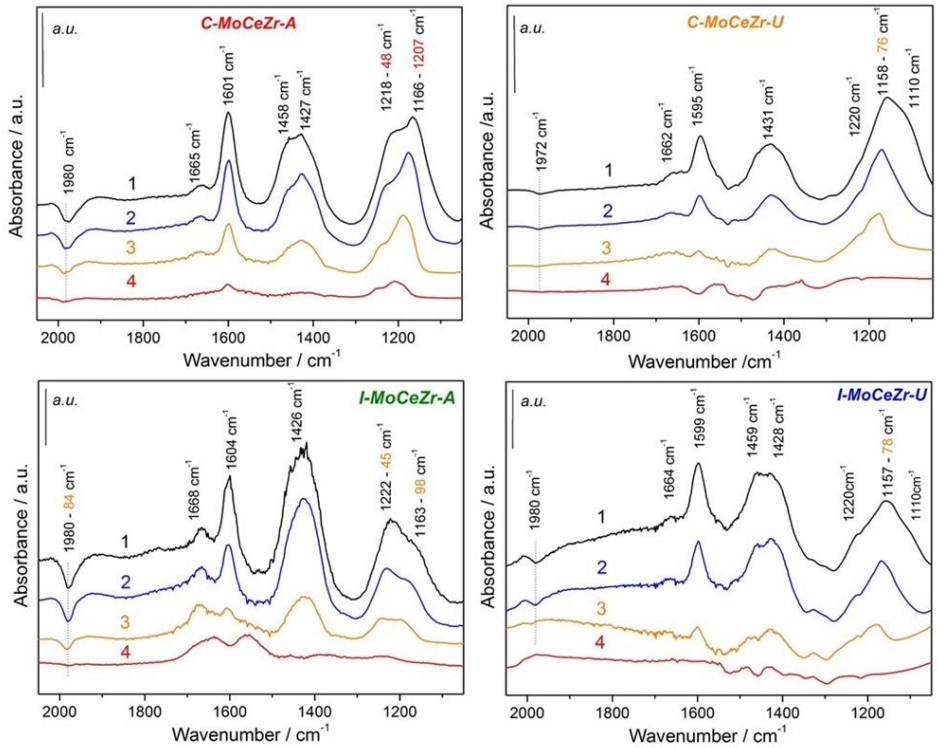
C-MoCeZr-A
a.u.
1980 cm-1
1665 cm-1
1601 cm-1
1458 cm-1
1427 cm-1
1218 - 48 cm-1
1166 - 1207 cm-1
C-MoCeZr-U
1972 cm-1
1662 cm-1
1595 cm-1
1431 cm-1
1220 cm-1
1158 - 76 cm-1
1110 cm-1
I-MoCeZr-A
1980 - 84 cm-1
1668 cm-1
1604 cm-1
1426 cm-1
1222 - 45 cm-1
1163 - 98 cm-1
I-MoCeZr-U
1980 cm-1
1664 cm-1
1599 cm-1
1459 cm-1
1428 cm-1
1220cm-1
1157 - 78 cm-1
1110cm-1
Absorbance / a.u.
Absorbance /a.u.
Wavenumber / cm-1
Wavenumber /cm-1
1
2
3
4
2000
1800
1600
1400
1200

Figure 89

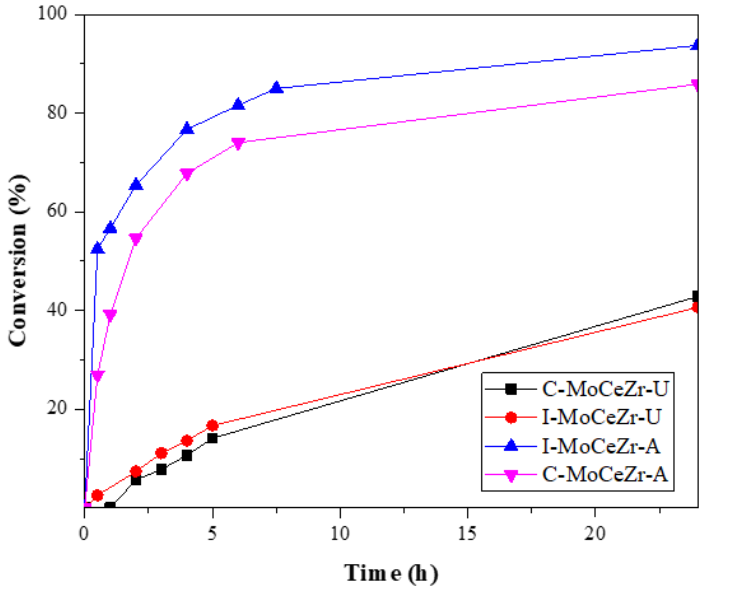

Figure 91